Synthesis and Characterization of Silica Coated CdSe/CdS Core/Shell Quantum Dots

Yang Xu

Dissertation submitted to the faculty of the Virginia Polytechnic Institute and State University in partial fulfillment of the requirements for the degree of

Doctor of Philosophy

In

Electrical Engineering

Dr. Kathleen Meehan
Dr. Louis J. Guido
Dr. Guoquan Lu
Dr. Chris L. Wyatt
Dr. Nancy G. Love

December, 2005
Blacksburg, Virginia

Keywords: CdSe, CdS, silica, quantum dot, semiconductor nanocrystal

Synthesis and Characterization of Silica Coated CdSe/CdS Core/Shell Quantum Dots

Yang Xu

Abstract

A great deal of interest has been dawn on the colloidal chemistry based semiconductor nanocrysallites, also known as quantum dots (QDs). Because of the strong quantum confinement, quantum dots have unique size-dependent optical properties, which are much more superior to the conventional organic fluorescence materials. In addition, strong chemical resistant makes inorganic semiconductor QDs ideal candidate for next-generation of bio-labels and drug delivery vehicles. This report presents a user friendly approach to synthesize high quality biocompatible CdSe QDs in aqueous solution. Size of the dots can be controlled by adjusting the temperature, pH of the solution, and ratio of the precursors. A thin CdS layer was grown on CdSe QDs, forming a CdSe/CdS core/shell structure, to improve the photoluminescence. In order to use these QDs *in-vivo*, a more chemically robust coating, silica, was grown on the core/shell structure QD. The optical properties of the QDs were characterized by absorption and photoluminescence spectra. X-ray diffraction and transmission electron microscopy were conducted to verify the QDs composition and structure.

Acknowledgements

I thank my parents, Yuan C. Xu and Pei Q. Wang, for raising me, guiding me and always being there through everything. I also own thanks to my wife, Chun H. Li, for her love and support. It is their encouragement and support that made me accomplish goals that I had thought impossible.

I would like to express my appreciation to my dissertation advisor, Dr. Kathleen Meehan, for her motivation, support and sharing of her expertise. Her guidance, patience and selflessness during the development of this work are greatly appreciated. I am also indebted to the assistance of my committee: Dr. Louis Guido, Dr. G.Q Lu, Dr. Chris Wyatt, and Dr. Nancy Love. Each of them has been very supportive to my efforts and desire to see this through.

Poojitha Mariam deserves many thanks for helping me to develop the first successful sample. Thanks to my co-workers, Guangyin Lei, Annette Booker, Nick Tacky, Yoshitaka Tada and Jess Calata for their valuable discussion and help.

For technical assistance, Mr. Steve McCartney and Mr. Li Yan deserve my appreciation for conducting the TEM and XRD experiments. Additional thanks are extended to Mr. Richard White and Dr. Sean Agnew at University of Virginia for their assistance of performing HRTEM and XRD sample scanning.

Contents

List of Tables

List of figures

Chapter 1 Introduction

Inorganic semiconductor nanocrystallites, also known as quantum dots, have been extensively studied by scientists and engineers over the past decades because of their unique size dependent optical properties (Murray, Norris et al. 1993), which are very different from their bulk counterparts because of quantum mechanical effects. A broad range of applications in many different disciplines for quantum dots have been proposed. These include their use as optoelectronic components (Bukowski and Simmons 2002) such as quantum dot lasers, IR photodetectors and display LEDs and as fluorescence labels in the life science (Michalet, Pinaud et al. 2005). Among the various compositions of quantum dots, CdSe quantum dots are the most interested materials as biomarkers for researchers in biology and medical science because the photoluminescence from the CdSe quantum dots can be tuned to covers almost all the visible wavelength (465nm – 640nm, from www.evidenttech.com), which is very important for visualizing the cells or tissues that are investigated.

In this study, high quality CdSe quantum dots were synthesized in aqueous solution. Gelatin was used as a capping agent to slow the chemical reaction so the CdSe dots would not grow too fast or form aggregations as well as to provide a biocompatible coating on the quantum dots so that they have potential to be used as *in-vivo* biosensors. A layer of CdS was grown around the CdSe dots to form a core/shell structure to enhance the photoluminescence of CdSe quantum dots since the higher band gap material will passivate the surface defects of CdSe dots and help to confine the electron-hole pair more in the CdSe core region. To make the CdSe/CdS core/shell structure quantum dots more resistant against photochemical reactions, a silica layer was grown on top of the CdS shell through surface silanization (D 2001; WCW, DJ et al. 2002). UV-Vis absorption and photoluminescence were carried out to characterize the optical properties of these quantum dots. X-ray diffraction (XRD) was conducted to identify the crystallographic structure of the core/shell and transmission electron microscopy (TEM) was performed to

confirm the shape and size distribution of the quantum dots.

The basic physics of quantum dot and their applications in life science are presented in Chapter 2, along with a review of some of the more commonly used synthesis methods. In Chapter 3, the experimental details of CdSe quantum dots synthesis process and a discussion of several effects on the formation of these dots are described. By varying the reaction temperature, pH value, and molar ratio of the solution, we found that the quantum dots synthesized with near neutral pH and 6:1 Cd^{2+} to Se^{2-} ratio at room temperature have the strongest photoluminescence. Chapter 4 focuses on the synthesis and characterization of CdSe/CdS core/shell structure. By coating the higher band gap semiconductor CdS, the photoluminescence of this CdSe/CdS core/shell structure are up to two times that obtained of the bare CdSe dots. However, we also found that there was a maximum thickness of the CdS. Due to the lattice mismatch between CdS and CdSe, thick CdS layer produces additional defects that quench the photoluminescence. Growth of the silica coating and its effect on CdS/CdSe quantum dots are discussed in Chapter 5. The silica coating provided CdS/CdSe quantum dots much stronger resistance to oxidation and Ostwald ripening. In addition, the quantum confined Stark effect was observed on the silica coated CdS/CdSe quantum dots. The engineering significance is presented in Chapter 6.

Reference

Bukowski, T. J. and J. H. Simmons (2002). "Quantum dot researh: current state and future prospects." Solid state and materials sciences **27**: 119-142.

D, G. (2001). "Synthesis and properties of biocompatible water-soluble silica-coated CdSe/ZnD semicounductor quantum dots." J. Phys. Chem. B **105**: 8861-8871.

Murray, C. B., D. J. Norris, et al. (1993). "Synthesis and Characterization of nearly monodisperse CdE (E=S, Se, Te) Semiconductor Nanocrystallites." J. Am. Chem. Soc. **115**: 8706-8715.

WCW, C., M. DJ, et al. (2002). "Quantum dots as luminescent probes in biological systems." Curr. Opin. Solid State Mater. Sci. **6**: 365-370.

Chapter 2 Background of Quantum Dots

2.1 Quantum Confinement in Semiconductors

Quantum dots (QDs) are nanometer-scale semiconductor crystallites. Since the size of the dots is much less than the exciton Bohr radius, the electron-hole pair in a quantum dot is tightly confined in all three dimensions, known as quantum confinement, which produces a number of pronounced modifications in the optical properties of the semiconductor.

To have a better understanding of quantum confinement, we will start with a discussion of the properties of the bulk materials. Semiconductors are often classified by the periodic table groups to which they belong. Table 2.1 lists some bulk phase physical properties of several common semiconductors, including their band gap energies, corresponding wavelengths, exciton Bohr radii, and exciton binding energies.

Table 2.1 Material Parameters for Several Common Semiconductors

Material	Periodic Table Classification	Band gap Energy (eV)	Band gap Energy (nm)	Exciton Bohr Radius (nm)	Exciton Binding Energy (meV)
CdS	II-VI	2.42	512	2.8	29
CdSe	II-VI	1.76	705	4.9	16
GaN	III-V	3.42	360	2.8	
GaP	III-V	2.26	550	10-6.5	13-20
InP	III-V	1.35	920	11.3	5.1
GaAs	III-V	1.42	870	12.5	5
AlAs	III-V	2.16	570	4.2	17
Si	IV	1.11	1150	4.3	15
Ge	IV	0.66	1880	25	3.6

Sources of data

GaN: (H.Morkoc 1999)

InP: (Cardona 1996)

Ge: (Smith, Pan et al. 1975)

AlAs: (Adachi 1985)

GaP: (Auvergne, Merle et al. 1975)

In bulk semiconductor materials, the energy levels of both conduction band and valence band are continuous, with electrons and holes moving freely in all directions. As the dimensions of the material shrink, effect of quantum confinement will easily be seen. Three different types of confinement that have been realized among inorganic semiconductors are described below.

2.1.1 Quantum Well

A quantum well (QW) is a sandwich structure with a thin layer of narrower band gap semiconductor in the middle of two layers of wider band gap semiconductor. There are two types of quantum wells. In a type I QW, a potential well, which confines the electrons and the holes in the narrower band gap material region, is formed between the narrower and wider band gap materials; while in a type II QW, the electrons and the holes are confined in different layers (see Figure 2.1).

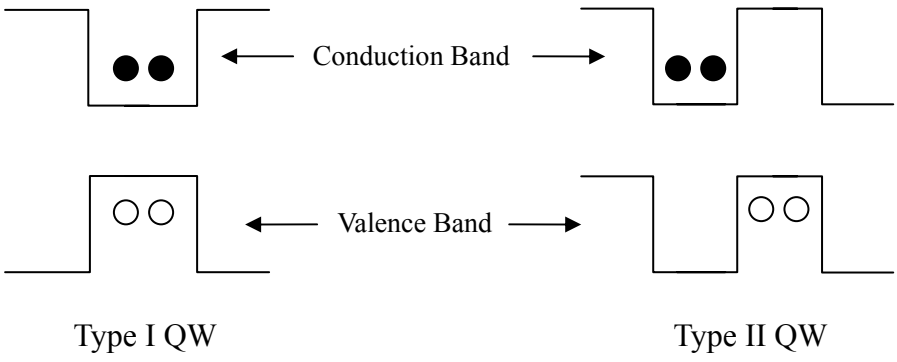

Figure 2.1 Illustration of type I and II quantum well

In a QW, the electrons and the holes can only move freely in two dimensions. The model of "*a particle in a one-dimensional-box*" can be used to provide a first description of the movement of the carriers. In the semiconductor, unlike the model, the potential barriers are finite and are determined by the difference in the band gaps of the two semiconductors and whether the alignment forms a type I or type II QW. Because of the finite value of the potential barrier, the wavefunctions of electrons and holes do not have to be zero at the boundaries. The wavefunctions extend into the wider band gap material, where they decay exponentially into this region. Also, the lowest energy band-to-band optical transition is not equal to the band gap of smaller band gap semiconductor. It is at a higher energy level determined by the difference between the lowest state of the electrons in the conduction band and the corresponding state of the holes in valence band. For electrons, the lowest energy level in a square potential well can be calculated as

$$E_j - E_c = \frac{h^2 j^2}{8m^* d^2} \tag{2.1}$$

where j is the quantum number labeling the level and d is the width of the potential well.

2.1.2 Quantum Wire

A quantum wire is a structure in which the electrons and holes are confined in two dimensions. Such confinement allows free electron and hole behavior in only one direction, along the length of the wire.

2.1.3 Quantum Dot

Typically of dimension ranging from 1 to 100 nanometers, a quantum dot has the most restricted confinement — in all three dimensions — of the electrons and holes. The dimension of a quantum dot is smaller than the de Broglie wavelength of thermal electrons, which is

$$\lambda = h/p = h/(2m_eE)^{1/2} = h/(2m_e\,kT)^{1/2} \approx 7.6\ nm \qquad (2.2)$$

where m_e is chosen to be equal to 9.1e-31 kg. An important property of a quantum dot is its large surface to volume ratio. The consequence of this feature is that QDs have pronounced surface-related phenomena.

2.1.4 Summary of Quantum Confinement Effects

Quantum confinement introduces a number of important modifications in the physical properties of semiconductors. A brief summary of the quantum confinement effects is presented below.

First of all, quantum confinement introduces an pronounced change in the density of states of semiconductor. The density of states *g(E)* is defined by the number of energy states between energy *E* and *E+dE*, which is derived by *dn(E)/dE*. For electrons in a bulk semiconductor, *g(E)* is zero at the bottom of the conduction band and increases as the energy of the electrons in the conduction band increases, given by $E^{1/2}$. This behavior is shown in Figure 2-2, which compares the density of states for electron in a quantum well (and also in quantum wire and dot), where the density of states is a step function because of the discreteness of the energy levels along the confinement direction.

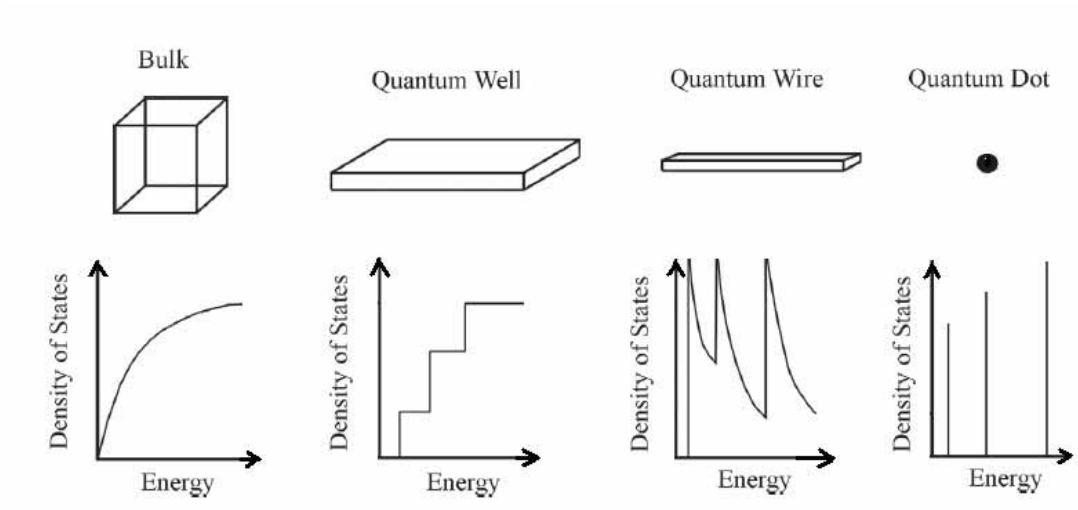

Figure 2.2 Density of states vs. energy for bulk material, quantum well, quantum wire and quantum dot

The density of states for a quantum wire has an inverse energy dependence $E^{-1/2}$. For each sub-band, the density of states has a large value near $k_z=0$ and decays as $E^{-1/2}$ as k_z has nonzero values for that sub-band. The energy levels for an electron in a quantum dot have only discrete values, which makes the density of states a series of delta functions at each of the allowed energy value, i.e. $g(E) = \delta(E-E_n)$ $(n=1, 2, ...)$. Theoretically, this feature gives sharp absorption and emission spectra for quantum dots even in room temperature.

Quantum confinement also induces a blue shift in the band gap and appearance of discrete sub-bands corresponding to energy quantization along the direction of confinement. The quantum mechanics description of this phenomenon will be presented later in this chapter. As the dimensions of the material increase, the energy of the confined states decreases so the inter-band transitions shift to longer wavelengths. When the dimensions of the material are greater than de Broglie wavelength, the inter-band transition energy finally approaches the bulk value.

As mentioned above, the density of states for both the valence and the conduction bands are significantly modified by quantum confinement. Instead of a smooth and continuous distribution of the density of states, the energy states are packed in a narrow energy range as the dimension of the material shrink. Discrete energy levels concentrate oscillator strength to the lowest level transitions. The oscillator strength of an inter-band optical transition depends on magnitude of the density of states in both the valence bands and the conduction bands. It also depends on the overlap of the wavefunctions of electrons and holes. Both factors produce a larger enhancement of oscillator strength with increasing quantum confinement in Type I semiconductors, and the oscillator strength is maximized for quantum dots, which are the most confined structures.

Intra-band transitions, also known as free carrier absorption in the bulk semiconductor, are electrons movements from one allowable energy to another within the conduction band or holes from one energy to another in the valence band. These transitions often depend on the presence of free carriers introduced by impurity doping or

charge injection by a bias field. In the bulk, because intra-band transitions from one k value to a different k value of conduction band require a change of quasi-momentum k, which could occur with lattice phonons coupling, these processes are usually much weaker than band-to-band transitions, which do not require a change of k. However, in quantum confined structures such as a quantum well, sub-bands exist that correspond to energy quantization along the direction of confinement. For the conduction band in a quantum well, an electron can shift from one sub-band to another without changing its two-dimensional quasi momentum k. These new transitions have been utilized to produce sub-band detectors and lasers, such as QWIPs (Levine 1993) and quantum cascade lasers (Faist, Capasso et al. 1996; Capasso, Faist et al. 1997).

Similar to the intra-band transition, an inter-band transition for indirect band gap material, such as silicon, also requires a change of quasi-momentum k and, thus, involves the phonon coupling. As a result, the emission of a photon produced by the transition of an electron from the conduction band to the valence band, known as recombination of electron and hole, is either extremely weak or nonexistent in the bulk form of an indirect gap semiconductor. Trap-assisted recombination could occur when an electron falls into a "trap", an energy level within the band gap introduced by the presence of a foreign atom or a structural defect. In a second step, the “trapped” electron moves into an empty valence band state to complete the recombination process. However, the traps are generally undesirable because they shorten the lifetime of carriers and produce multiple energy pathways which contribute to non-radiative recombination. While in the quantum confinement structures, quasi momentum uncertainty Δk is increased because position uncertainty of electrons Δx is reduced by the confinements, according to the “uncertainty principle”. The relaxed quasi momentum Δk selection rule, then, allows enhanced emission to be observed in some indirect band gap material, such as porous silicon (Canham 1997) and silicon nanoparticles (Belomoin, Therrien et al. 2002).

Band gaps of bulk semiconductors can be altered by many factors, such as temperature and stress by applied mechanical force. The most noticeable among these is the Stark effect, which is the change of the electrical properties and the optical spectra due to the modified energy band structure by an applied electric field. In quantum

confinement structures, such as a quantum well, if an electric field is applied along the confinement direction, the binding energy of the exciton decreases as the electric field pushes the electron and the hole wavefunctions to opposite sides of the confined region (Figure 2.3). The electric field can also mix different quantized states and, therefore, the oscillator strength redistributes between optically allowed (such as $1S_{3/2}1S_e$) and optically forbidden (such as $1P_{3/2}1S_e$) excited states through matrix element

$$W_{sp} = <1S_{3/2}1S_e \ |erF|1P_{3/2}1S_e> \tag{2.3}$$

where *er* is the electric dipole operator and *F* is the electric field. The combination of all these effect is called quantum confinement Stark effect. The quantum confinement Stark effect on the quantum dots conducted in this study will be discussed in Chapter 5.

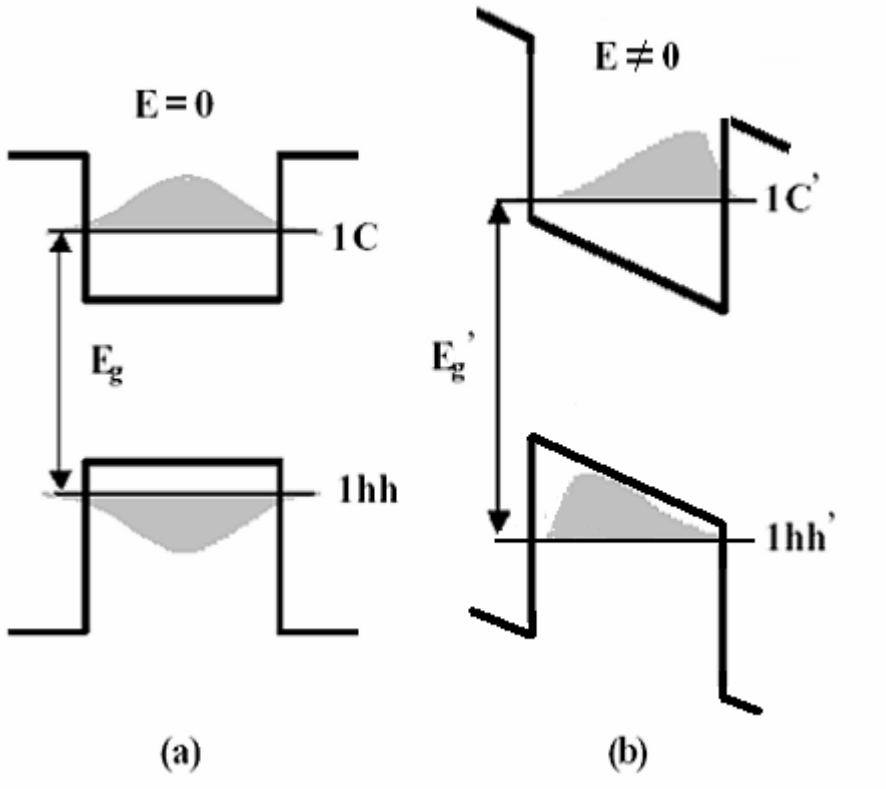

Figure 2.3 Quantum confinement Stark effect

2.2 Basic Physics of Quantum Dots

In order to have a better understanding of the size dependent optical properties of quantum dots, a basic quantum mechanics description of optical transitions observed in quantum dots is necessary.

Real semiconductor band structures are quite complicated and can only be calculated with computational methods. However, a simple yet sufficient model, the "*effective mass approximation*", simplifies the band structures as parabolic forms near either bottom of conduction bands or top of valence bands (Manasreh 2005). The bulk wavefunction, $\Psi(r)$, according to Bloch's theory, can be written as

$$\Psi(r) = u_{nk}(r)\ exp(ikr) \tag{2.4}$$

where u_{nk} is a function with the periodicity of crystal lattice and the wavefunctions are labeled by the band index n and wavevector k. Due to the parabolic forms of the bulk band structures, the energy of both conduction and valence bands can be written as

$$E_c = \frac{\hbar^2 k^2}{2m_{eff}^c} + E_g \tag{2.5}$$

$$E_v = -\frac{\hbar^2 k^2}{2m_{eff}^v} \tag{2.6}$$

where E_g is the semiconductor band gap and energies are relative to the top of the valence band. In this model, the carriers act as free particles with an "effective mass", m_{eff}, which incorporates the periodic potential felt by the carriers.

If one can assume that the diameters of quantum dots are much larger than the lattice constant of the material, the "*envelop function approximation*" then allows us to write the single particle (electron or hole) wavefunction as Bloch function (Manasreh 2005). To satisfy the boundary condition, which requires the wavefunction equals zero outside the quantum dots, the single particle wavefunction can be written as a linear

combination of Bloch function

$$\Psi(r) = \sum_k C_{nk} u_{nk}(r) \exp(ikr) \tag{2.7}$$

If the functions u_{nk} weakly depend on k, then Equation (2.7) can be rewritten as

$$\Psi(r) = u_{n0}(r) \sum_k C_{nk} \exp(ikr) = u_{n0}(r) f(r) \tag{2.8}$$

where *f(r)* is the single particle envelop function. The periodic function u_{n0} can be written as a combination of atomic wavefunctions φ_n in the "*tight-binding approximation*" (Manasreh 2005).

$$u_{n0}(r) = \sum_i C_{ni} \varphi_n(r - r_i) \tag{2.9}$$

where the sum is over lattice sites. After the functions u_{n0} are determined, the quantum dot problem is now left to construct the envelop functions for the single particle wavefunctions, *f(r)*.

So far, we have completely overlooked the Coulomb interaction between the electron and the hole, which could generate an exciton in bulk materials. To justify the neglect of this interaction in quantum dots, "*strong confinement approximation*" has to be applied (Manasreh 2005). Because the Coulomb interaction and the confinement energy are proportional to $1/r$ and $1/r^2$, respectively, in real small space, such as within a quantum dot, the confinement energy is much larger than the Coulomb interaction. So we can add Coulomb term as a first order energy correction, E_c.

This way, the quantum dot problem can be solved by a "*particle in a sphere*" solution (Manasreh 2005). The simple "*particle in a sphere*" model treats a particle in a potential sphere with radius a_0, where the potential is zero inside the sphere and is equal to infinity outside.

By solving Schrödinger equation, the wavefunction can be written as

$$\Phi(r,\theta,\phi) = C\,\frac{j_l(k_{nl}r)Y_l^m(\theta,\phi)}{r} \tag{2.10}$$

where is the $Y_l^m(\theta,\phi)$ spherical harmonic, $j_l(k_{nl}r)$ is the l^{th} order of spherical Bessel function with $k_{nl} = \frac{\alpha_{nl}}{a_0}$. The energy of the particle is given by

$$E_{nl} = \frac{\hbar^2\alpha_{nl}^2}{2m_0a_0^2} \tag{2.11}$$

which is proportional to $1/a_0^2$ and, therefore, depends on the size of the particle. Combining equations (2.8) and (2.11), the electron-hole pair states can be written as

$$\Psi_{eh} = u_c f_c(r) u_v f_v(r) = C\left[u_c\,\frac{j_l(k_{nl}r_c)Y_l^m}{r_c}\right]\left[u_v\,\frac{j_l(k_{nl}r_v)Y_l^m}{r_v}\right] \tag{2.12}$$

with energies given by

$$E_{eh}(n_hL_hn_eL_e) = E_g + \frac{\hbar^2}{2a_0^2}\left(\frac{\varphi_{n_hL_h}^2}{m_{eff}^v} + \frac{\varphi_{n_eL_e}^2}{m_{eff}^c}\right) - E_c \tag{2.13}$$

These states are labeled as $n_hL_hn_eL_e$.

Although the conduction and valence bands are described as simple parabolic bands in the "*particle in a sphere*" model, the real band structure of II-VI semiconductor, such as CdSe, is more complicated. The conduction band in CdSe crystal with wurtzite structure can still be approximated as a single parabolic band, while the valence band is 6-fold degenerate at *k=0*. This degeneracy is removed due to the strong spin-orbit coupling and the valence band is split into two sub-bands, $p_{1/2}$ and $p_{2/3}$ ($J = l + s$, *l=1, s=1/2*), at *k=0*. For nonzero values of k, the $p_{2/3}$ sub-bands becomes $J_m = \pm 3/2$ and $\pm 1/2$

sub-bands. These sub-bands are often referred as heavy-hole, light-hole and spin-off sub-bands (Figure 2.4a). The degeneracy of heavy-hole and light-hole sub-bands at *k=0* is lifted by the crystal field due to the asymmetric lattice structure (Figure 2.4b).

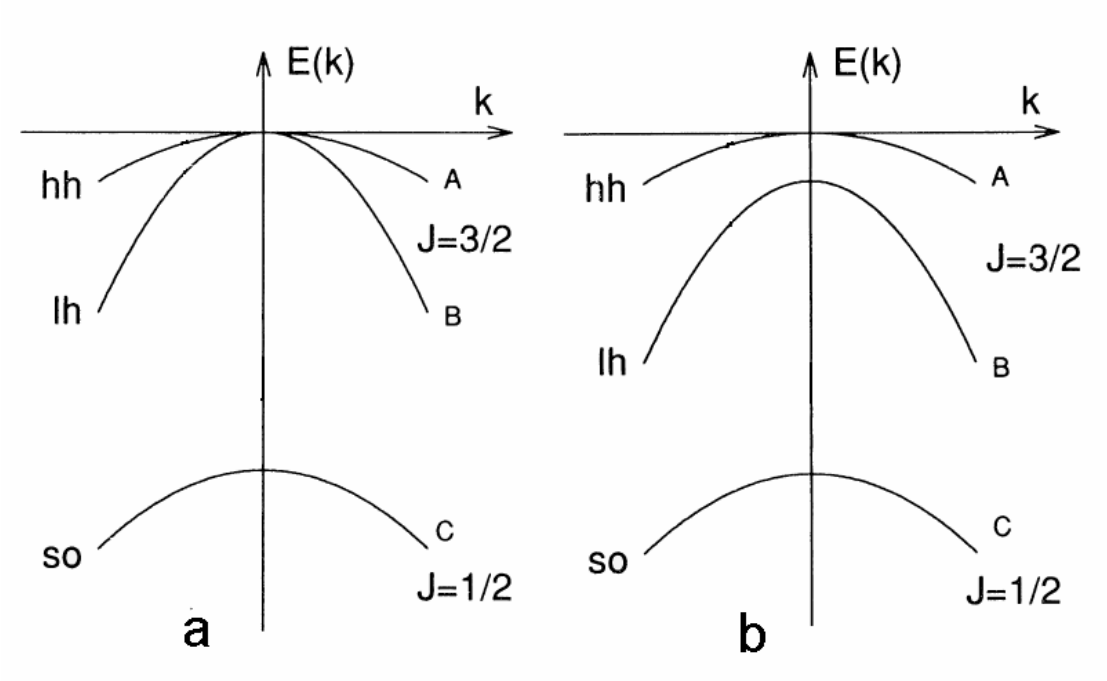

Figure 2.4 Illustration of valence band structure near *k=0*

The optical transition probability of the given quantum dot state pair is described by the dipole matrix element

$$P = \left| \left\langle \Psi_e \left| ep \right| \Psi_h \right\rangle \right|^2 \tag{2.14}$$

where the *e* is the polarization vector of the light.

Because the momentum vector p only acts on the unit cell portion of wavefunction and the envelop functions vary little over this length, equation (2.14) can be rewritten after substituting in equation (2.11)

$$P = \left|\langle u_c \left| ep \right| u_v \rangle\right|^2 \left|\langle f_e \left| f_h \right. \rangle\right|^2 \tag{2.15}$$

Due to the orthonormality of the envelop functions in "*particle in a sphere*" model, equation (2.15) yields

$$P = \left|\langle u_c \left| ep \right| u_v \rangle\right|^2 \delta_{n_e n_h} \delta_{L_e L_h} \tag{2.16}$$

thus, the selection rule, $\Delta n = 0$ and $\Delta L = 0$, can be acquired.

2.3 Applications of Quantum Dots in Life Science

Due to their strong size dependent optical properties, quantum dots have been explored extensively in many aspects of applications, which are covered by a number of reviews (AJ 2002; WCW, DJ et al. 2002; A, X et al. 2003; WJ, D et al. 2003; X and S 2003; P 2004; Parak, Pellegrino et al. 2005). However, the discussion here will only focus on the applications in life science.

In cell biology, it has been a common practice to use organic fluorophores as molecular labels or to identify structural compartments in order to observe the molecules or organelles under an optical microscope, which is a very important technique used to investigate the cellular processes in living cells. Otherwise, the cells are almost transparent to visible light and, therefore, direct observation of any cell activity is hardly possible. These fluorophores can be attached to the target directly or to some molecule (such as antibodies), which binds to the target. Although such labeling techniques are widely used today, the limitations of the conventional fluorophores are obvious. A well known phenomenon associated with organic fluorophores is photobleaching (B and E 1994), in which irreversible light-induced photochemical reactions happen to the fluorophores. As a result, these organic molecules become non-fluorescent soon after having been illuminated with the excitation light. Different color fluorophores are generally different organic molecules, so it is difficult to handle them all in experiments that require multicolor imaging due to the chemical property difference among each type

of molecules. Organic fluorophores also have narrow excitation wavelength windows and broad emission bands so the set of fluorophores used and the excitation source and detection system have to be carefully chosen to obtain strong signals without significant optical overlap between fluorophore emissions. Other drawbacks of organic fluorophores, such as pH dependent of the fluorescence efficiency and biochemical interference with regular cell activity, make them far less attractive compared to the new nanomaterial-based fluorescence labels. Colloidal metal nanoparticles, such as gold, have been used as bio-labels (J and J 2003). These tiny metal particles do not photobleach and offer strong contrast under electron microscopy, such as transmission electron microscopy (TEM), which has much better resolution than optical microscopy. However, TEM requires stable or fixed samples, which means the samples have to be dead before any observations can be made.

In the past decade, quantum dots have been highlighted as bio-labels since they offer many advantage over the traditional fluorophores. First of all, these inorganic materials are more robust against photobleaching than organic molecules (Parak, Pellegrino et al. 2005). This is particularly important for experiments that require observations with extended period of time. In fact, this benefit has already been successfully demonstrated in many practical labeling processes (Parak, Boudreau et al. 2002; Pellegrino, Parak et al. 2003). Secondly, since the photoluminescence wavelength of quantum dots are determined by their size, multicolor imaging can be conducted with same material of different sizes (Rosenthal, Tomlinson et al. 2002). Also, complexity of sample preparation is limited because their surface properties are defined by the coating material. In addition, quantum dots have broad absorption spectra and narrow emission bands so it is possible to excite different dots with single light source and the emissions from one sized quantum dot can be easily distinguished from that of another sized quantum dot. Another advantage of quantum dots is their long fluorescence lifetime, which is on the order of a few tens of nanoseconds. In contrast, the fluorescence lifetime of organic fluorophores is about a few nanoseconds, the same as many biological samples' auto-fluorescence. Thus, by using time delayed detection system, fluorescence signal from quantum dots can be recorded virtually free of background noise (Dahan,

Laurence et al. 2001).

High quality inorganic semiconductor nanomaterials, such as CdSe, CdS, CdTe or CdSe/ZnS, have been synthesized via different approaches (Murray, Norris et al. 1993; Dabbousi, Rodriguez-Viejo et al. 1997; Peng and Peng 2001; Qu, Peng et al. 2001), among which the synthesis method with organic solvent at high temperature is the most popular. Although the surfactants used in this method are hydrophobic, these quantum dots can still be made hydrophilic after surface modification. Exchange of the hydrophobic coatings with ligand molecules are the most commonly used approach (Winter, Liu et al. 2001; Sukhanova, Devy et al. 2004). These ligand molecules carry functional groups that can link to the quantum dots surface on one end and hydrophilic groups on the other end. The most frequently used groups reactive to the surface of quantum dots are thiol (–SH) functionalities, and carboxyl (–COOH) functionalities are most often used as hydrophilic head groups. Another approach is to grow a silica coating around the quantum dots through surface silanization (D 2001; WCW, DJ et al. 2002), which has been conducted in this study and will be discussed in Chapter 5. It has been demonstrated that the silica coating make the quantum dots extremely stable in the solution (Zhou, Kobayashi et al. 2004). Coating the quantum dots with amphiphilic polymers, such as octylamine-modified poly(acrylic acid) (PAA), have also been reported recently (Pellegrino, Manna et al. 2004; Petruska, Bartko et al. 2004). Instead of surfactant exchange, the whole quantum dot is covered by the special polymers regardless of what is already around the dot.

To be used as bio-labels, quantum dots still have to be functionalized. Since thiol group (-SH) binds with the most commonly used quantum dots material, such as CdSe, CdS and ZnS, the target biological molecules with thiol group can be conjugated with these dots by partial ligand exchange, which means some of the hydrophilic surfactant are substituted by the target molecules. One of the problems of this type of conjugation is the stability of the connection between quantum dots target molecules as the “thiol to semiconductor” bonds are not very strong. Another approach to link quantum dots with target molecules is covalent bonding. Most of the quantum dots have negative charge on the surface, therefore the positively charged molecules can

attach to the dots non-specifically by ionic bonding. Successful conjugations between quantum dots and a variety of biological molecules, such as biotin (Bruchez, Moronne et al. 1998), folic acid (WCW, DJ et al. 2002) and DNA (Pathak, Choi et al. 2001; Gerion, Parak et al. 2002; Parak 2002; Schroedter, Weller et al. 2002; Gerion, Chen et al. 2003), have been reported by many groups. It has also been proven that the functions of target molecules do not change significantly once they are attached by quantum dots (Zhang 2000).

After the demonstration of quantum dots as fluorescence labels for molecules, researchers began to bring the application of these quantum dots to a new higher level, incorporating the quantum dots into the living cells and tissues. Depending on the ligand attached to the quantum dots, they can be either naturally up taken by the cells or injected into the cells with microinjection techniques. Once inside the cells, these functionalized dots can act as the reporter of the biochemical reaction inside the cells or the cell development itself, such as embryonic development, which could answer questions like how an embryo can develop into a complete fully functional organism. Ability to trace a cell migration in animal/human body is another interesting question need to be revolved in cancer study. If the quantum dots can be incorporated into cancer cells and made to be optically and chemically stable for a sufficiently long period of time, they will help researchers to monitor these cells moving from one place to another. Quantum dots have also been proposed as drug delivery vehicles that could initiate certain photo-activated chemical reactions (www.in-pharmatechnologist.com 2005; Ozkan 2004). Despite the advantages of quantum dots, large scale production and the potential toxicity of these dots in human body remain to be resolved.

2.4 Synthesis Methods of Quantum Dots

Depending on their applications, high quality quantum dots of various semiconductor materials have been synthesized either on a substrate or dispersed in (organic/inorganic) solution. Some of the major methods used to fabricate quantum dots are described in this section.

2.4.1 Epitaxial Growth Techniques

Molecular Beam Epitaxy (MBE) is a widely used technique for epitaxial growth of quantum-confined structures of both II-VI and III-V compound semiconductors as well as silicon and germanium. The growth is carried out in an ultrahigh vacuum chamber, where the atoms that are the constituents of the semiconductors to be grown are evaporated by heating the effusion cells or ovens. The vapor passes through a small orifice, accelerated by the pressure differential on two sides of the orifice, and, thus, forms a molecular beam. Because of the low density of this molecular beam, the particles neither react nor collide with each other before they impinge on the substrate mounted on the opposite side of the chamber. By monitoring and controlling the fluxes from different cells together with the substrate temperature, the composition and the epitaxial growth rate on the substrate can be precisely controlled. The ultra high vacuum chamber in MBE allows the use of many in situ analytical techniques to characterize the condition of the substrate surface prior to growth and the crystallinity, composition, and thickness of the epitaxial material. The MBE technique is well suited for fabrication of quantum wells, quantum wires and quantum dots. The quantum well growth can be precisely controlled layer by layer. The fabrication of quantum wires and quantum dots can be realized by using substrates with a patterned surface. Another form of quantum dot array, three-dimensional islands on a substrate, can be synthesized when there is a large strain between a thin epitaxial layer and the substrate due to a significant lattice mismatch between the two materials. The surface reconstruction, facilitated by the substrate temperature, results in the formation of three-dimensional structures, composed of the epitaxial material at regular spacing across the surface of the substrate. MBE technique has revolutionized the semiconductor technologies and widely used in manufacturing semiconductor laser diodes and quantum dot laser diodes, which involve MBE-growth quantum well and quantum dot structures.

Metal-organic chemical vapor deposition (MOCVD) is another commonly used epitaxial growth method in which the semiconductor structure are grown from the

precursors of metal organics and hydrides. In a MOCVD process, the suitable precursors of semiconductor in gas form are transported to the reaction chamber, and then deposition and growth of the semiconductor take place on a substrate. Finally, the remaining decomposition products are removed from the chamber. Self-assembled GaN quantum dots were grown on the $Al_xGa_{1-x}N$ surfaces using a surfactant has been reported (Tanaka, Iwai et al. 1996). Generally, MOCVD offers the advantage of being a simple and faster growth technique, with a growth rate typically 10 times that of MBE. However, the precursors are highly toxic and, thus, require extreme safeguard and care during handling. In addition, the hydrodynamic condition of gas flow does not permit the extensive in situ characterization.

Another technique to grow quantum dots on a substrate that have evolved in recent years is laser-assisted vapor deposition (LAVD), in which the deposition materials ablated by lasers are directly deposited onto the substrate or mixed with a reactive gas to produce the appropriate material (Ventra, Evoy et al. 2004).

2.4.2 Colloidal Synthesis of Quantum Dots

An alternative approach is to produce quantum dot in solutions, called colloidal synthesis, which deals with chemical reactions in solution on a nanometer scale. Colloidal synthesis has been conducted to make semiconductor nanostructures of different composition, size and shapes. This method involves growing nanoparticles of inorganic materials through chemical reaction of their precursors and, sometimes, controlled precipitation of the reaction product in certain solvents. Generally, the growth process starts with the fast formation of a huge number of nuclei. Then more and more of the solid product deposits onto the nuclei, so the sizes of the crystallites grow slowly till the desired size is reached, at which time the reaction must be quenched. Otherwise, the dots could keep growing under a process, known as Ostwald ripening, which is the growth of larger dots through the transfer of material from smaller ones, which have a higher solubility.

CdSe quantum dot has been the most frequently produced semiconductor

nanocrystallite due to its unique PL spectra. One of the most popular synthesis methods for CdSe quantum dot is organometallic approach. In a general synthesis process, dimethyl cadmium and selenium powder dissolved in trioctylphosphine are the precursors for Cd and Se, respectively. Trioctylphosphine oxide (TOPO) is used as reaction solvent and heated up to 300°C in an oxygen free environment. Then, the liquid precursors are rapidly injected into the reaction chamber (Murray, Norris et al. 1993). CdSe nanocrystallites immediately begin to nucleate and grow. The desired size of CdSe quantum dots can be achieved by adjusting the amount of injected precursors and the reaction time. Although high quality of quantum dots have been produced since early 90s by this method, the expensive and extremely toxic materials used is this process and hard-to-controlled reaction condition motivate scientists to explore more user-friendly approaches to make quantum dots. CdO, a safer reactant, as Cd precursor has been used to produce CdTe and CdSe QDs (Peng and Peng 2001; Qu and Peng 2002). Since the quantum dots used in bio-applications need to be hydrophilic and the process of substitute of hydrophobic ligands with water-soluble coatings could be laborious, new aqueous-based CdSe QDs synthesis techniques have been developed in recent years. Peng, et al. have made CdSe QDs with elemental-direct-reaction (Peng, Dong et al. 2001); Yan, et al. produced QDs through photon-irradiation (Yan, Li et al. 2003). In the present study, a detailed method of preparing CdSe quantum dot in aqueous solution is described in next chapter.

A prerequisite in utilizing quantum dots as biolabels is that they remain stable in the colloidal suspension, i.e. they do not grow so large or aggregate that they precipitate. There are several stabilization mechanisms to prevent precipitation of quantum dots. One of them is electrostatic stabilization, which involves the creation of a double layer of ions around the dots resulting in a Coulombic repulsion among close dots. Another mechanism is steric stabilization, which uses a hydrophilic or amphiphilic polymer, like polyethyleneglycol (Parak 2002) or dextrane (Wilhelm 2003), to coat the quantum dots. The considerable space, occupied by polymer molecules, keeps the dots getting close to each other. Scientists also use micelles, which are formed by lipids or other amphiphilic molecules and have a hydrophilic exterior, to encapsulate quantum dots for stabilization

(Dubertret, Skourides et al. 2002; Fan, Leve et al. 2005).

High quality quantum dots used in biological applications have been exclusively prepared by advanced colloidal chemistry over the past decades. Different approaches to stabilize QDs in aqueous solution have been proposed and realized. As part of the present study, an evaluation of protein and organosilica coatings to stabilize the quantum dots was performed.

Reference

A, W., W. X, et al. (2003). "Lighting up cells with quantum dots." Biotechniques **34**: 296-300.

Adachi, S. (1985). "GaAs, AlAs and AlxGa1-xAs: Material Parameters for Use in Research and Device Applications." J. Appl. Phys. **58**(3): R1-R29.

AJ, S. (2002). "Quantum dots as luminescent probes in biological systems." Solid State Mater. Sci. **6**: 365-370.

Auvergne, D., P. Merle, et al. (1975). "Phonon-Assisted Transitions in Gallium Phosphide Modulation Spectra." Phys. Rev. B **12**(4): 1371-1376.

B, P. J. and C. V. E (1994). "Practical laser-scanning confocal light microscopy: obtaining optimal performance from your instrument Cell Biology—A Laboratory Handbook." 44-64.

Belomoin, G., J. Therrien, et al. (2002). "Observation of a magic discrete family of ultrabright Si nanoparticles." Appl. Phys. Lett. **80**: 841.

Bruchez, M., M. Moronne, et al. (1998). "Semiconductor Nanocrystals as Fluorescent Biological Labels." Science **281**: 2013.

Canham, L. (1997). "Properties of Porous Silicon."

Capasso, F., J. Faist, et al. (1997). "Infrared (4–11 μm) quantum cascade lasers." Solid State Communications **102**: 231-236.

Cardona, P. Y. Y. a. M. (1996). Fundamentals of Semiconductors. New York, Springer-Verlag.

D, G. (2001). "Synthesis and properties of biocompatible water-soluble silica-coated CdSe/ZnS semiconductor quantum dots." J. Phys. Chem. B **105**: 8861-8871.

Dabbousi, B. O., J. Rodriguez-Viejo, et al. (1997). "(CdSe)ZnS Core-Shell Quantum Dots: Synthesis and Characterization of a Size Series of Highly Luminescent Nanocrystallites." J Phys Chem B **101**: 9463.

Dahan, M., T. Laurence, et al. (2001). "Time-gated biological imaging by use of colloidal quantum dots." Optics Letter **26**: 825-827.

Dubertret, B., P. Skourides, et al. (2002). "In Vivo Imaging of Quantum Dots Encapsulated in Phospholipid Micelles." Science **298**: 1759-1762.

Faist, J., F. Capasso, et al. (1996). Appl. Phys. Lett. **68**: 3680-3682.

Fan, H., E. W. Leve, et al. (2005). "Surfactant-Assisted Synthesis of Water-Soluble and Biocompatible Semiconductor Quantum Dot Micelles." Nano Lett. **5**: 645-648.

Gerion, D., F. Chen, et al. (2003). "Ultra-fast room-temperature single nucleotide polymorphism detection and multi-allele DNA detection using fluorescent nanocrystal probes and microarray." Anal. Chem. **75**: 4766-4772.

Gerion, D., W. J. Parak, et al. (2002). "Sorting fluorescent nanocrystals with DNA." J Am. Chem. Soc. **124**: 7070-7074.

www.in-pharmatechnologist.com (2005). "Nanotechnology to revolutionize drug delivery."

H.Morkoc (1999). Nitride Semiconductors and Devices. New York, Springer-Verlag.

J, K. A. and K. J (2003). "Electron microscopy in cell biology: integrating structure and function." Nat. Cell Biol. **5**: ss6-10.

Levine, B. F. (1993). J. Appl. Phys. **74**: R1.

Manasreh, O. (2005). "Semiconductor Heterojunctions and Nanostructures."

Murray, C. B., D. J. Norris, et al. (1993). "Synthesis and Characterization of nearly monodisperse CdE (E=S, Se, Te) Semiconductor Nanocrystallites." J. Am. Chem. Soc. **115**: 8706-8715.

Ozkan, M. (2004). "Quantum dots and other nanoparticles: what can they offer to drug discovery?" Drug Disc Today **9**: 1065-1071.

P, A. (2004). "The use of nanocrystals in biological detection." Nat. Biotechnol. **22**: 47-52.

Parak, W. J. (2002). "Conjugation of DNA to silanized colloidal semiconductor nanocrystaline quantum dots." Chem. Mater. **14**: 2113-2119.

Parak, W. J., R. Boudreau, et al. (2002). "Cell motility and metastatic potential studies based on quantum dot imaging of phagokinetic tracks." Adv. Mater. **14**: 882-885.

Parak, W. J., T. Pellegrino, et al. (2005). "Labeling of cells with quantum dots." Nanotechnology **16**: R9-25.

Pathak, S., S. K. Choi, et al. (2001). "Hydroxylated quantum dots as luminescent probes for in situ hybridization." J Am. Chem. Soc. **123**: 4103-4104.

Pellegrino, T., L. Manna, et al. (2004). "Hydrophobic Nanocrystals Coated with an Amphiphilic Polymer Shell: A General Route to Water Soluble Nanocrystals." Nano Lett. **4**: 703-707.

Pellegrino, T., W. J. Parak, et al. (2003). "Quantum dot-based cell motility assay." Differentiation **71**: 542-548.

Peng, Q., Y. Dong, et al. (2001). Inorg. Chem. **40**: 3840.

Peng, Z. A. and X. Peng (2001). "Formation of High-Quality CdTe, CdSe, and CdS Nanocrystals Using CdO as Precursor." J Am. Chem. Soc. **123**: 183.

Petruska, M. A., A. P. Bartko, et al. (2004). "An Amphiphilic Approach to Nanocrystal Quantum Dot-Titania Nanocomposites." J Am. Chem. Soc. **126**: 714-715.

Qu, L., Z. A. Peng, et al. (2001). "Alternative Routes toward High Quality CdSe Nanocrystals." Nano Lett. **1**: 333-337.

Rosenthal, S. J., I. Tomlinson, et al. (2002). "Targeting cell surface receptors with ligand-conjugated nanocrystals." J Am. Chem. Soc. **124**: 4586-4594.

Schroedter, A., H. Weller, et al. (2002). "Biofunctionalization of Silica-Coated CdTe and Gold Nanocrystals." Nano Lett. **2**: 1363-1367.

Smith, D. L., D. S. Pan, et al. (1975). "Impact Ionization of Excitons in Ge and Si." Phys. Rev. B **12**(10): 4360-4366.

Sukhanova, A., J. Devy, et al. (2004). "Biocompatible fluorescent nanocrystals for immunolabeling of membrane proteins and cells." Anal. Biochem. **324**: 60-67.

Tanaka, S., S. Iwai, et al. (1996). "Self-assembling GaN quantum dots on AlxGa1-xN

surfaces using a surfactant." Appl. Phys. Lett. **69**: 4096-4098.

Ventra, M. D., S. Evoy, et al. (2004). "Introduction to nanoscale science and technology."

WCW, C., M. DJ, et al. (2002). "Quantum dots as luminescent probes in biological systems." Curr. Opin. Solid State Mater. Sci. **6**: 365-370.

Wilhelm, C. (2003). "Intracellular uptake of anionic superparamagnetic nanoparticles as a function of their surface coating." Biomaterials **24**: 1001-1011.

Winter, J. O., T. Y. Liu, et al. (2001). "Recognition Molecule Directed Interfacing Between Semiconductor Quantum Dots and Nerve Cells." Adv. Mater. **13**: 1673-1677.

WJ, P., G. D, et al. (2003). "Biological applications of colloidal nanocrystals." Nanotechnology **14**: R15-27.

Wu, X., H. Liu, et al. (2003). "Immunofluorescent labeling of cancer marker Her2 and other cellular targets with semiconductor quantum dots." Nat. Biotechnol. **21**: 41-46.

Ventra, M. D., S. Evoy, et al. (2004). "Introduction to nanoscale science and technology."

X, G. and N. S (2003). "Molecular profiling of single cells and tissue specimens with quantum dots." Trends Biotechnol. **21**: 371-373.

Yan, Y. L., Y. Li, et al. (2003). "Preparation and characterization of CdSe nanocrystals via Na2SO3-assisted photochemical route." Materials Science and Engineering **B103**: 202-206.

Zhang, C. Y. (2000). "Quantum dot-labeled trichosanthin." Analyst **125**: 1029-1032.

Zhou, X., Y. Kobayashi, et al. (2004). "Preparation of silica encapsulated CdSe quantum dots in aqueous solution with the improved optical properties." Applied Surface Science **242**: 281-286.

Chapter 3 Synthesis and Characterization of CdSe Quantum Dots

3.1 Introduction

Due to the quantum confinement of electrons and holes in all three dimensions, semiconductor nanocrystals or quantum dots (QDs) with dimensions smaller than the bulk exciton Bohr radius show interesting size-dependent electronic and optical properties (Murray, Norris et al. 1993; Alivisatos 1996; Woggon 1997). Currently, II-VI semiconductor nanocrystals are under extensive investigation as emitting materials for thin-film light emitting devices (Colvin, Schlamp et al. 1994; Tessler, Medvedev et al. 2002), optical amplifier media for telecommunication networks (Harrison, Kershaw et al. 2000), low-threshold lasers (Klimov, Mikhailovsky et al. 2000), and biological labels (Bruchez, Moronne et al. 1998; Dubertret, Skourides et al. 2002). Recent studies have indicated that chemical bonding of attached ligands can be detected through changes in the photoluminescence signal from the QDs, which will enable them to be used in a similar manner as molecular beacons (Dwarakanath, Bruno et al. 2004; Kim, Morikis et al. 2004; Lin, Joseph et al. 2004). CdSe nanocrystals are also excellent candidates for multicolor fluorescence imaging in biology applications (Bruchez, Moronne et al. 1998; Chan and Nie 1998; Michalet, Pinaud et al. 2005) because the photoluminescence (PL) spectra of different sized CdSe quantum dots cover much of the visible wavelength range (from 450 nm to 650 nm) with a spectral width on the order of 30 nm (Huang, Chen et al. 2004).

In order to exploit CdSe QDs in these potential applications, the photoluminescence efficiency must be high; thus, high quality nanocrystals have to be synthesized. Numerous synthesis techniques have been developed by researchers from around the world; much of this research has concentrated on organometallic synthesis techniques. Dimethyl cadmium $Cd(CH_3)_2$ has long been adopted as a precursor for the synthesis of high quality cadmium chalcogenides QDs (Murray, Norris et al. 1993;

Murray, Kagan et al. 2000; Peng, Manna et al. 2000; Donega, Hickey et al. 2003). However, the extremely toxic organometallic materials that are used in this process overshadow their benefits. CdO has been recently reported as a safer reagent to make Cd-based chalcogenide nanocrystals (Peng and Peng 2001; Qu and Peng 2002). Unfortunately, the temperature at which the reaction occurs is still high (250~300ºC). In addition, the hydrophobic nature of the ligands on the QDs produced using the now conventional organometallic approach prevents them from being applied directly for *in-vivo* applications. The techniques to substitute the original ligand coatings with hydrophilic coatings are quite complex (Henshaw, Parkin et al. 1996; Wang, Zhang et al. 1999). More straightforward routes to synthesize CdSe QDs directly in aqueous solutions via photo-irradiation (Yan, Li et al. 2003) and by elemental-direct-reaction (Peng, Dong et al. 2001) have been developed. The reaction temperature for these processes is much reduced from that used in organometallic synthesis of quantum dots but at a cost of significantly longer process times. Nonetheless, the results from these studies provided the motivation to explore simple and relatively fast techniques to synthesize CdSe quantum dots that employ nontoxic coatings, which are compatible with *in-vivo* applications.

Here we report on an easy and low cost method to prepare high quality CdSe quantum dots in aqueous solution, where gelatin was used as an inhibitor. UV-Vis absorption and PL spectra were acquired in order to characterize the optical properties of QDs. A qualitative example of the difference between the two measurements is shown in Figure 3.1. The vials contained different sized CdSe nanoparticles. Visible light was used to illuminate the solutions of colloidal CdSe in Figure 3.1A and the colors observed are a result of the strong absorption by the CdSe of the green and blue photons. Ultraviolet (UV) light was used to illuminate the solutions in Figure 3.1B, which caused the quantum dots to fluorescence. As discussed earlier in Chapter 2, the wavelength of photoluminescence (PL) is determined by the size of the QDs. The red, yellow and green color of the three samples in Figure 3.1B represent CdSe QDs with about 7nm, 3nm and 2.3nm, respectively, in diameter.

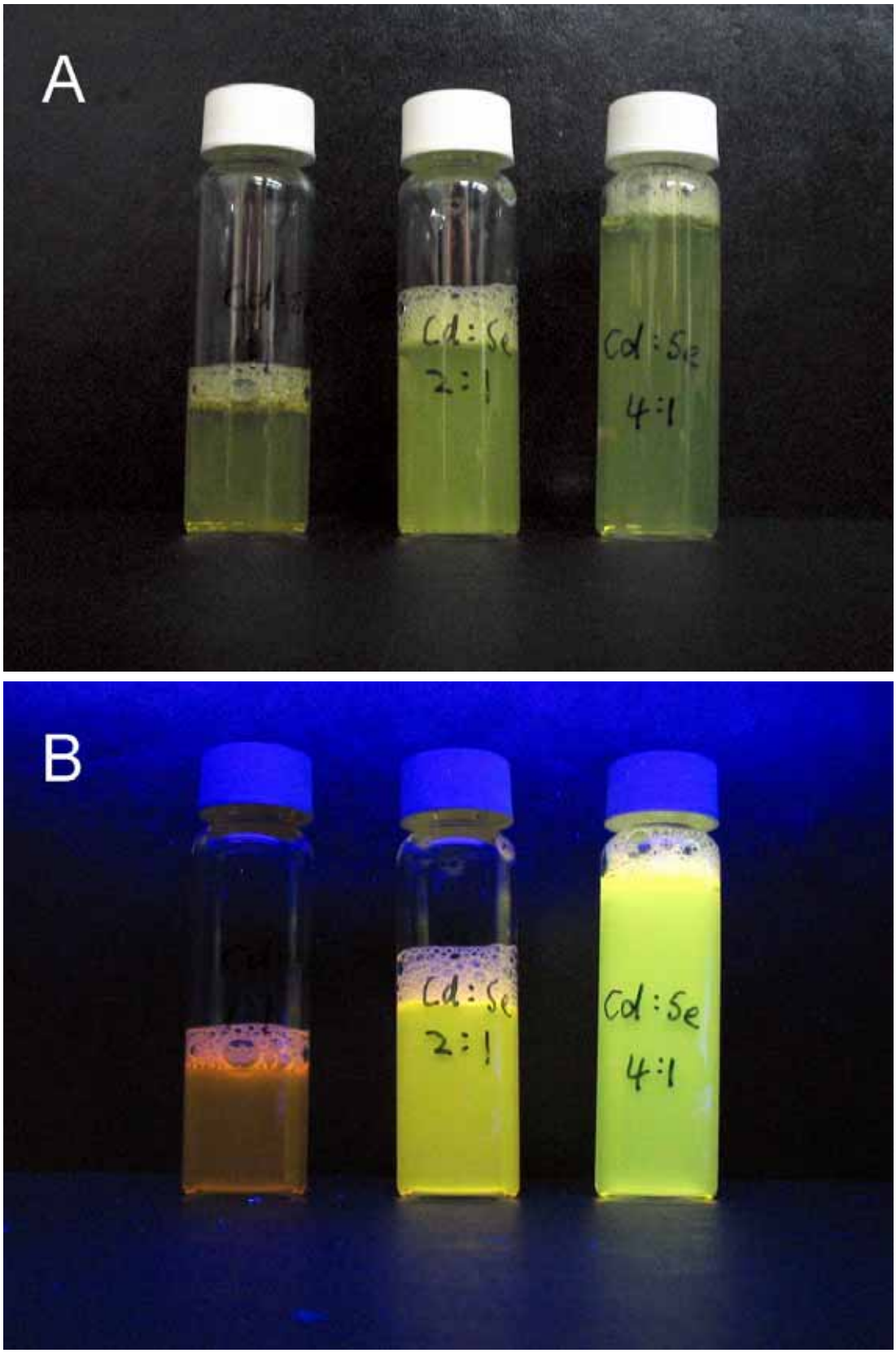

Figure 3.1 CdSe quantum dots with three different sizes A. illuminated with room light B. illuminated with UV light

The dimensions of the QDs were estimated from both the PL and absorption spectra. The QDs were then imaged using transmission electron microscopy (TEM) to confirm the size

3.2 Experiment Details

All the chemicals used were of analytical grade and deionized (DI) water (18.3 MΩ) was used in all the experiments. Sodium selenosulfate solution was prepared by heating appropriate amounts of selenium (99.999%, Cerac) and sodium sulfite (98+%, Acros) in deionized water at 80^{o}C for an hour and final solution was adjusted to 20 mM (Solution 1). 0.8 mM of $CdCl_2$ (99%, Acros) and 0.1 g of gelatin (type A) were added to 20 ml of DI water (Solution 2). In order to completely dissolve the gelatin, the mixture was put into a water bath at 50ºC for 5 minutes. After Solution 2 was allowed to cool down to room temperature, ammonium hydroxide (Tetra metal grade, Seastar Chemical Inc.) was added to adjust the pH of the solution to the required level. Solution 2 and Solution 1 were then mixed in different molar ratios and agitated continuously at room temperature until the quantum dots were formed. The color of the solution ranged from light green to orange, depending on the size of the quantum dots produced. The resulting solutions were centrifuged to remove the excess gelatin before optical characterization of the QDs was performed.

Absorption spectra were obtained using a Shimadzu UV-Vis spectroscopy system. Photoluminescence of the quantum dots was carried out at an excitation wavelength of 450 nm with a fluorescence spectrometer that was assembled using two Spex 1680 monochrometers, a tungsten light source, and an R928 multi-alkali photomultiplier tube. The absorption spectra present in this paper were confirmed by repeating the process at least three times and the photoluminescence spectra scan were repeated more than ten times during this study. The TEM was performed using a Philips EM420T transmission electron microscope. The sample preparation consisted of placing a small droplet of the diluted solution on a carbon thin film-coated TEM grid, which was dried in open air.

The grid was then loaded into the TEM to obtain the images of the QDs.

3.3 Results and Discussion

Typical absorbance and PL spectra of the QD solutions are shown in Figure 3.2. The high energy shoulder at around 500 nm in the absorbance spectrum indicates the size of the QD is about 2 nm (Murray, Norris et al. 1993). This was confirmed using TEM, as shown in Figure 3.3.

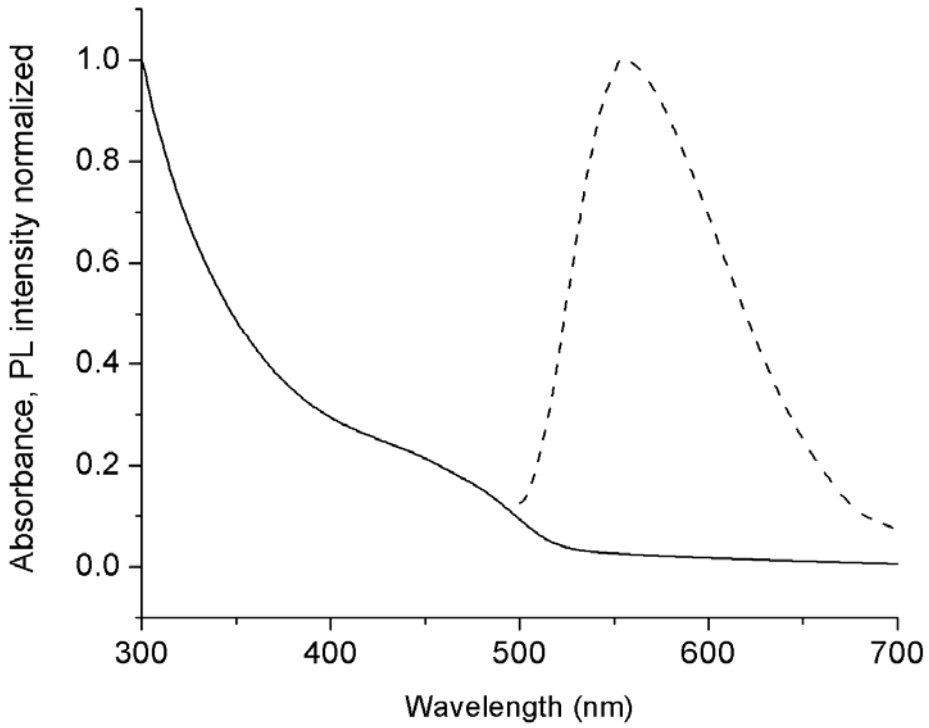

Figure 3.2 Typical absorbance (solid line) and PL (dashed line) spectra of the CdSe quantum dots solutions, in which the peak of each curve has been normalized to 1.0

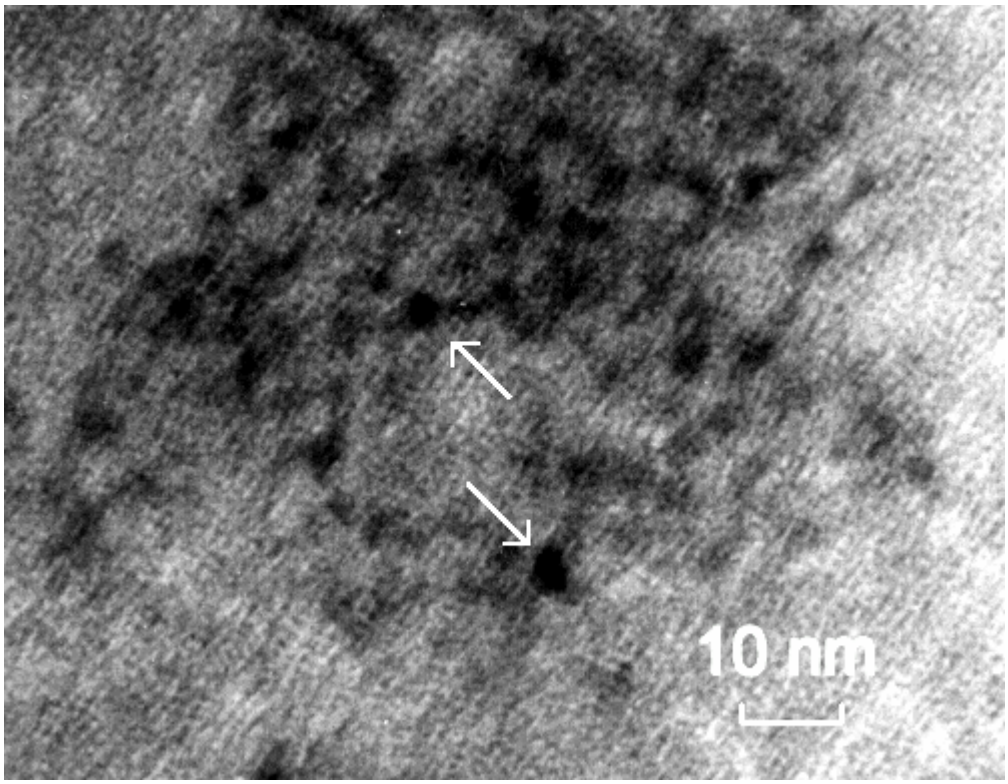

Figure 3.3 TEM micrograph of CdSe QDs at 50°C, pH8, molar ratio of Cd^{2+}/Se^{2-} 4:1 with 0.1g gelatin in 20 ml DI water

As described by Kainthla et al. (Kainthla, Pandya et al. 1980), $Cd(OH)_2$ is formed when ammonium hydroxide is added to the $CdCl_2$ solution. The $Cd(OH)_2$ begins to precipitate when the solubility product of $Cd(OH)_2$ in the solution is exceeded.

$$2NH_3 + 2H_2O + Cd^{2+} = Cd(OH)_2 + NH_4^+ \quad (3.1)$$

The $Cd(OH)_2$ precipitate dissolves in excess ammonia solution to form the complex cadmium tetra-ammonium ions $[Cd(NH_3)_4^{2+}]$

$$Cd^{2+} + 4NH_3 = Cd(NH_3)_4^{2+} \quad (3.2)$$

The hydrolysis of sodium selenosulfate in alkaline solution gives Se^{2-} ions

according to the equations:

$$Na_2SeSO_3 + OH^- = Na_2SO_4 + HSe^- \quad (3.3)$$

$$HSe^- + OH^- = H_2O + Se^{2-} \quad (3.4)$$

Supersaturation (S) of the ions over CdSe can be defined as the ratio between ionic solubility product (IP) of Cd^{2+} and Se^{2-} concentrations and the solubility product (SP) of CdSe.

$$S = IP / SP = [Cd^{2+}][Se^{2-}]/[CdSe] \quad (3.5)$$

In the presence of excess Cd^{2+} ions, cadmium selenide will form in the solution when the supersaturation is greater than one (Kainthla, Pandya et al. 1980; Woggon 1997).

$$Cd^{2+} + Se^{2-} = CdSe \quad (3.6)$$

In our experiment, gelatin was used as an inhibitor to control the reaction rate and stabilize the QDs in solution. The diffusivity of the Cd^{2+} and Se^{2-} ions was decreased in the solutions containing the gelatin because the viscosity of the solution with gelatin was greater than that of the solutions without gelatin. Thus, the presence of the gelatin limits the growth rate of the QDs. There are indications that the gelatin also limits the maximum size of the QDs during the initial stages of growth, preventing the formation of large crystals of CdSe, and inhibits the aggregation of quantum dots. The size of the QDs synthesized was stable if the solutions with gelatin were stored at 10°C; however, at room temperature, the effects of Ostwald ripening of the QDs were observed. A thick CdSe precipitate rapidly formed in the absence of gelatin.

3.3.1 Effect of Temperature

While maintaining the $CdCl_2$ solution (Solution 1) at pH 8 and the molar ratio between Cd^{2+} and Se^{2-} at 4:1 when Solutions 1 and 2 are mixed, the reactions were

carried out for 30 minutes at three different temperatures: 20°C, 50°C, and 90°C. 90°C was chosen because the previously reported studies used similarly high temperatures (Huang, Chen et al. 2004), 50°C because that was the temperature used to dissolve the gelatin, and room temperature was selected as it reduces the complexity of the synthesis process. As it is clear from the spectra presented in Figure 3.4, the largest dots were produced at 90°C while the strongest PL signal was obtained from the QDs synthesized at 20°C.

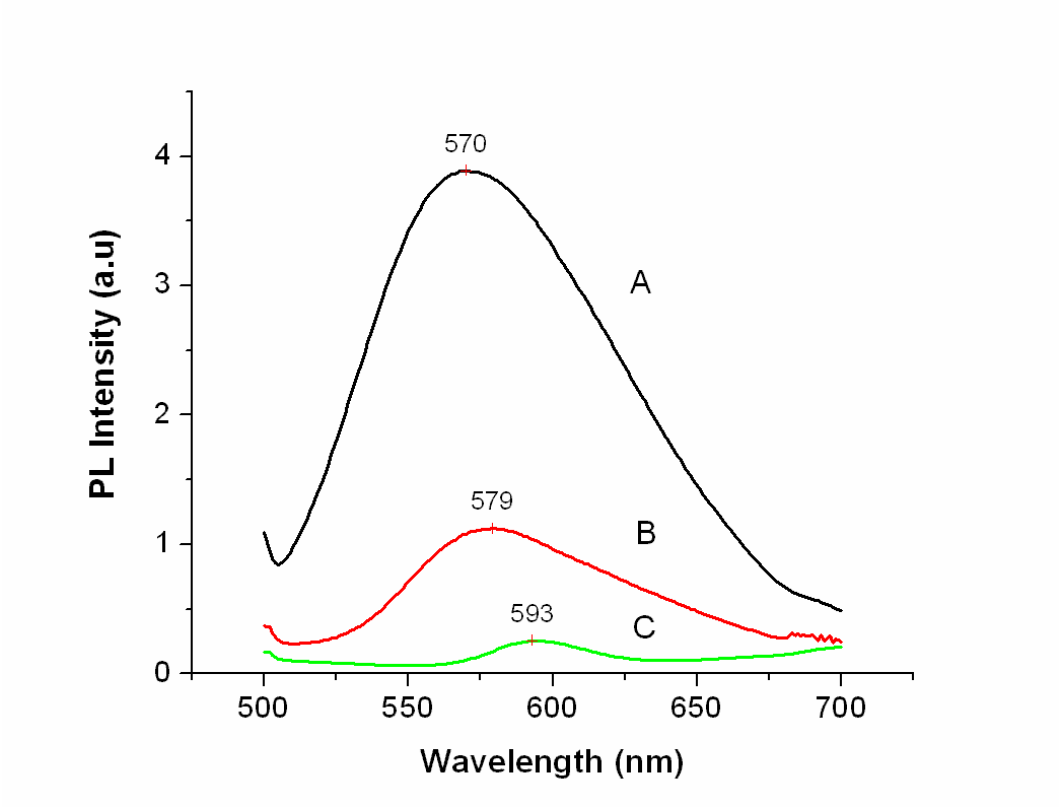

Figure 3.4 PL intensity as a function of wavelength at different temperatures A. 20°C B. 50°C and C. 90°C

The dissociation of the cadmium tetra-ammonium complex and selenosulphate depends on temperature (Kainthla, Pandya et al. 1980). At higher temperatures, the dissociation is greater, which produces higher concentrations of Cd^{2+} and Se^{2-} ions in the solution. Also, the increased kinetic energy of the ions at the higher temperatures

results in more frequent collisions so that the probability of CdSe quantum dots formation increases. Furthermore, the viscosity of the solution decreased as the synthesis temperature increased, allowing the Cd^{2+} and Se^{2-} ions to more readily diffuse within the solution, which also contributed to an increase in growth rate. However, PL intensity decreased with increasing growth rate of the nanocrystal. It is likely that the density of defects incorporated within and at the surface of the QDs increased as the growth rate increased, which results in more nonradiative recombination sites. This would explain the decrease in PL intensity at higher temperatures.

Taking into account the application of QDs in cell imaging, which requires high PL efficiency and small diameter dots with a narrow size distribution, 20°C was chosen as the optimum temperature to conduct further analysis of the synthesis process. Unless specified, all of the experiments described below were conducted at room temperature.

3.3.2 Effect of Different Molar Ratios of the Solutions

During this experiment, the concentration of Cd^{2+} and Se^{2-} ions in the final solution is adjusted by changing the volume of Solution 2 while holding the volume of Solution 1 constant. The Cd^{2+}:Se^{2-} ratios indicated are the molar ratios of the Solution 2 ($CdCl_2$) to Solution 1 (Na_2SeSO_3). As is shown in Figure 3.5, higher PL intensity of the solution is recorded by increasing the molar ratio of $CdCl_2$ to Na_2SeSO_3 from 2:1 to 6:1. It is also noticed that there was a significant difference in dimensions of the quantum dots when a transition in the synthesis conditions was made from a molar ratio of 6:1 to 2:1, but that changing the molar ratio from 6:1 to 4:1 has a negligible effect on the size of the dots.

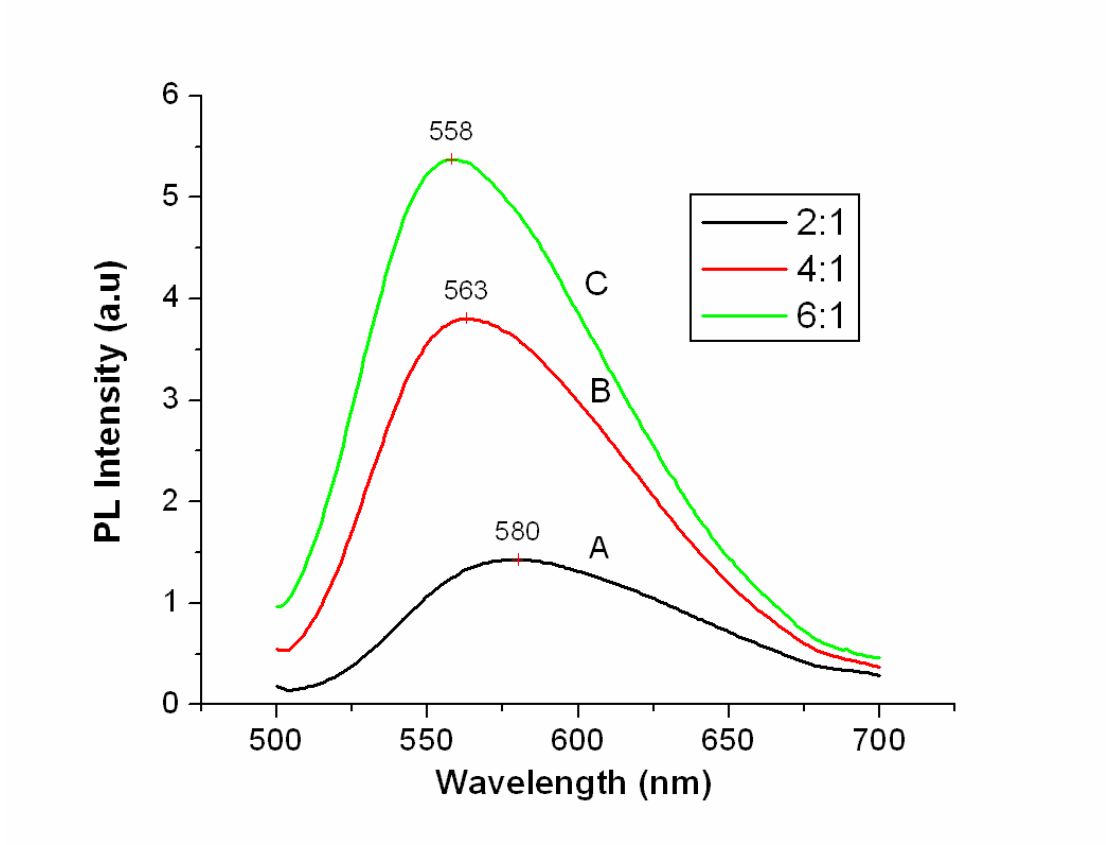

Figure 3.5 PL intensity as a function of wavelength at different molar ratios between Cd^{2+} and Se^{2-} ions at pH 8 and room temperature: A. 2:1, B. 4:1 and C. 6:1

In reaction rate-limited processes, the rate of the chemical reaction is proportional to the concentration of the reacting species and, thus, is a function of the supersaturation the solution. As the molar ratio of Cd^{2+}:Se^{2-} is increased, the ionic solubility product, IP, and, hence, the supersaturation, S, remains unchanged because the concentration of Cd^{2+} increased by the same magnitude as the concentration of Se^{2-} decreased in the solution. Thus, one would expect there to be no change in the nucleation and growth rates of the QDs. However, this analysis neglects the impact of the gelatin, the concentration of which increased as the Cd^{2+}:Se^{2-} ratio is increased. The absorbance of the QDs synthesized with a Cd^{2+}:Se^{2-} ratio of 2:1 is significantly larger than that obtained from the QDs synthesized with a Cd^{2+}:Se^{2-} ratio of 6:1. This implies that the increased concentration of gelatin impedes the reaction between Cd^{2+} and Se^{2-} to form CdSe by decreasing the mobility of the ions in solution, driving the reaction towards a diffusion-limited case. Moreover, the PL intensity from the QDs synthesized with a

Cd^{2+}:Se^{2-} ratio of 6:1 is much greater than that of the QDs synthesized with a Cd^{2+}:Se^{2-} ratio of 2:1. This implies that the individual CdSe QDs synthesized in the presence of a high concentration of gelatin have higher quantum efficiency as compared to those synthesized in the presence of a lower concentration of gelatin. It is not known whether the improved radiative efficiency is a result of fewer surface states or reduced defects within the QDs synthesized in the presence of a high concentration of gelatin.

3.3.3 Effect of pH

In order to examine the effect of pH on the properties of the quantum dots, $CdCl_2$ solutions of pH 7.2, 8 and 10 were prepared. Figure 3.6A and 3.6B illustrates the changes in the peak wavelength and intensity of the photoluminescence, respectively, as a function of molar ratio of $CdCl_2$ and Na_2SeSO_3 for three different pH solutions. Reactions performed at a pH of 7.2 produced smaller quantum dots as compared to pH 8 and 10. The PL intensity of the solutions was also found to be greater for lower pH values. The concentration of quantum dots in the pH of 7.2 solutions is lower compared to that obtained when the pH of Solution 1 was adjusted to 8, based upon absorbance data. When the PL intensity obtained from similar volumes of CdSe QDs in the aqueous solution was compared, it was consistently higher from the QDs in the pH 7.2 solutions than that obtained from the QDs in the pH 8 and pH 10 solutions. Therefore, we conclude that the QDs synthesized using the Solution 1 adjusted to a pH 7.2 yields more efficient CdSe quantum dots.

In this study, we also tried to lower the pH value of Solution 1 with hydrochloride acid before mixed with Solution 2. However, the sodium selenosulfate did not survive in acidic environment. Therefore, no QDs were able to be synthesized in this case.

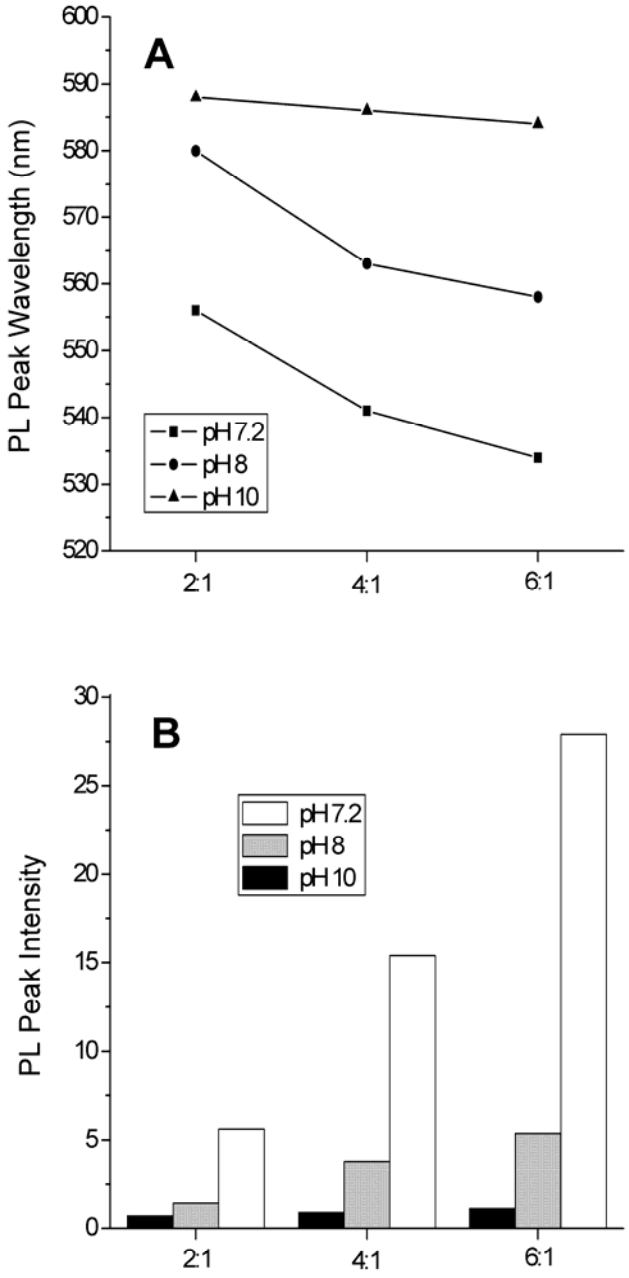

Figure 3.6 Peak wavelength and B. peak intensity of the PL from the QDs as a function of the molar ratio of Cd^{2+}:Se^{2-} at different pH values

The rate of formation of the quantum dots also depends on the supersaturation. The lower the supersaturation, the slower is the formation of CdSe. As the pH of the

$CdCl_2$ solution is increased, the concentration of Cd^{2+} and OH^- ions increases. Thus, the supersaturation increased, which will increase the growth rate (Kainthla, Pandya et al. 1980; Woggon 1997) of the CdSe QDs. This likely resulted in an increase in the density of nonradiative defects in the nanocrystals, which reduces the quantum efficiency of the QDs.

3.3.4 Effect of Gelatin Concentration

The effect of gelatin concentration on the size of the quantum dots is shown in Figure 3.7. Precipitation of $Cd(OH)_2$ was observed when ammonium hydroxide was added to $CdCl_2$ solution without gelatin. This indicated that the presence of the gelatin increased the solubility of the $Cd(OH)_2$ in Solution 1. This results in an increase in the supersaturation of the mixture of Solution 1 and Solution 2, resulting in growth of larger nanocrystals. Although the solution with 0.05g of gelatin in 20 ml DI water produced smaller sized nanocrystals than produced when 0.1g of gelatin was used, a considerable amount of precipitation of the CdSe was observed when left at room temperature for 3-4 hours. Thus, the lower concentration of gelatin was unable to stabilize the QDs in solution for any length of time. However, the viscosity of the CdSe QDs solutions with the highest concentration of gelatin proved to be too large to allow microinjection of the CdSe nanocrystals directly into cells, rendering these solutions useless for the *in-vivo* application. Since the excess gelatin can be removed by centrifuging the solution for 5-10 minutes at 10,000 rpm prior to the microinjection of the QDs, the high concentrations of gelatin during CdSe nanocrystal synthesis did not pose a problem. Therefore, 0.1g of gelatin in 20 ml of DI water was used to increase the shelf life of the solution. A fellow undergraduate researcher was trying to synthesize CdSe using sodium citrate as an inhibitor. He observed a rapid reduction, usually less than twenty minutes, in PL efficiency of his QDs. Compared to the several-days-long shelf life of the QDs synthesized with gelatin, we concluded that the surface oxidation process was significantly reduced by gelatin coating.

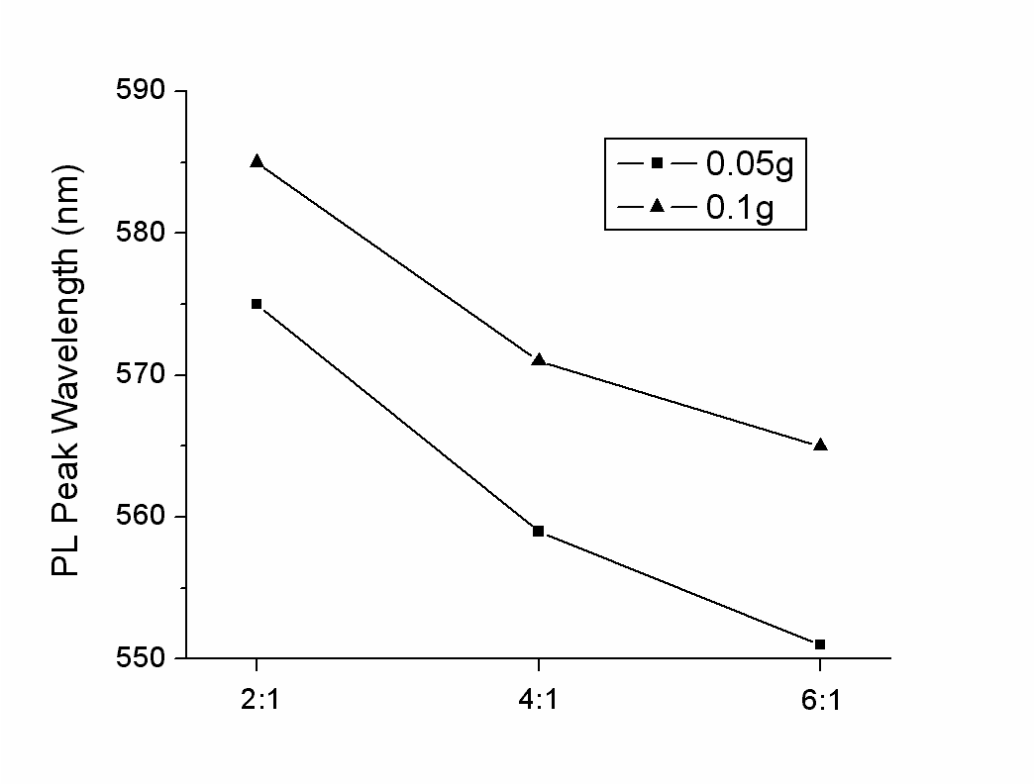

Figure 3.7 Peak PL wavelength from the QDs as a function of the molar ratio of Cd^{2+}:Se^{2-} with two concentrations of gelatin at pH 8

3.3.5 Photon Induced Quantum Dots Growth

An interesting phenomenon, photon induced quantum dots growth, was observed during the characterization. "U" shape silicone glue was applied on the edge of a 1cm x 1cm glass slide. Another same size slide was then placed on top of the glue and let dry over night (Figure 3.8). So the gap between the two slides is defined by the thickness of the glue (~1mm). The space between the slides was filled with CdSe quantum dots solution and the whole fixture was mounted on a filter holder. Light of different visible wavelengths from a 200W tungsten bulb were selected by a monochrometer and shined through the CdSe solution.

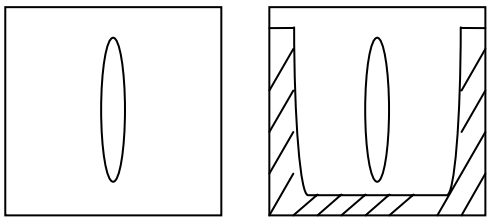

Figure 3.8 The fixture was made of two 1cm x 1cm slides, the shaded area indicates the silicone glue used to stick the two slides and the oval area is the region being illuminated

Three samples from the same CdSe solution were prepared and illuminated by 400nm, 450nm and 500nm photons, respectively, for 30 minutes. Digital photos of each sample were taken every 10 minutes. As can be observed from the images shown in Figure 3.9, there was a marked change in the color and opacity of the illuminated region.

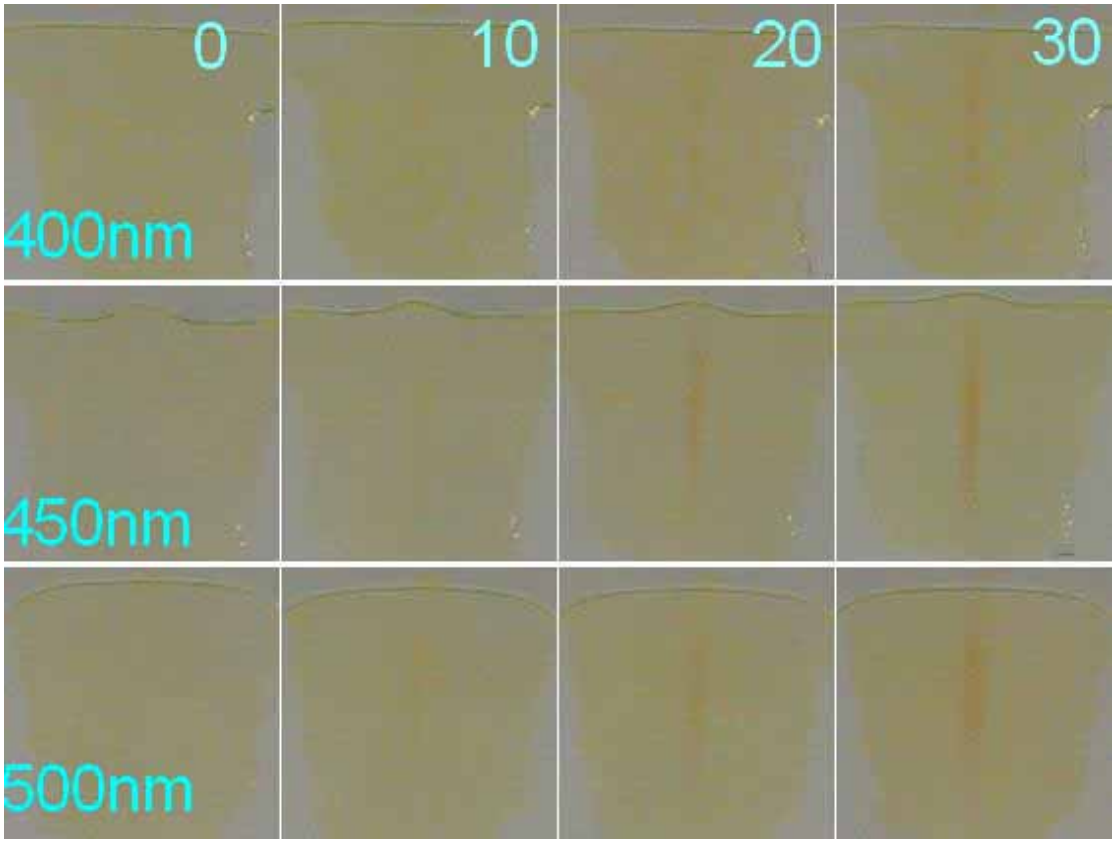

Figure 3.9 Light induced quantum dots growth

The darker area in the middle of each sample indicates the place where the collimated light shined through. It is clear from Figure 3.9 that the quantum dots had grown bigger in those areas.

Photon induced chemical reactions to form CdSe quantum dots has been reported by several groups (Nemec, Mikes et al. 2000; Yan, Li et al. 2003). It is believed that the electron-hole pair is created upon photon absorption in the nanocrystals. Because the hole is able to transfer into the solution, which leaves the dot negatively charged, a electrochemical reaction would take place on the charged dot (Hodes 1993). This is further supported by the fact that no photon induced growth was observed in a similar experiment conducted with the excitation wavelength at 600nm, which is below the absorption edge of the quantum dot solution and, thus, no electron-hole pair was created. Although the nonradiative recombination of the electron-hole pair could lead to localized heat generation, which is calculated to be on the order of several mK over the illuminated area, compared to the effect of the photochemical reaction initiated by the charge transfer in the solution, the effect of temperature rise on the generation of the bigger dots (as described earlier in this chapter) can be neglected.

3.4 Summary

High quality water soluble CdSe QDs were synthesized using gelatin as an inhibitor. The diameter of the quantum dots synthesized ranged from 2-7nm. The size of the dots synthesized was observed to increase when the supersaturation of the solution was increased, which occurred with increases in one or more of the process parameters: temperature, pH of Solution 1, and the molar ratios of the Cd^{2+} to Se^{2-} ions. It was found that there was a higher concentration of QDs in solution when the Cd^{2+}:Se^{2-} ratio was 2:1 as compared to 6:1, but the radiative efficiency of the individual QDs in solution with Cd^{2+}:Se^{2-} ratio of 6:1 is higher. Both effects are attributed, not to a change in the supersaturation, but to the increased concentration of gelatin in the solution. In a second experiment, larger diameter quantum dots were synthesized in solutions in which the gelatin concentration and the supersaturation were both increased. The increased gelatin concentration was also found to increase the stability of the quantum dots in solution,

reducing the rate at which Ostwald ripening occured with the subsequent CdSe precipitation from the solution. The reaction conditions of room temperature, a Solution 1 pH of 7.2, and a 6:1 molar ratio of Cd^{2+}:Se^{2-} with 0.1g gelatin in 20 ml of DI resulted in the synthesis of the smallest diameter nanocrystals (~2nm) with greatest radiative efficiency per nanocrystal. Finally, photon induced quantum dot growth was observed in the CdSe samples prepared in this study. This could be one more factor, among others, that contribute to the size of the quantum dots during the synthesis process, since all of the synthesis runs in this work were performed in fume hoods with fluorescent lighting. The photochemical reactions observed also indicates that organic molecules-capped CdSe quantum dots, gelatin capping in this case, are still relatively chemical reactive. Thus, there is a need for other coatings for the CdSe so that these QDs are more robust and chemically resistant.

Reference

Alivisatos, A. P. (1996). J. Phys. Chem. **100**: 13226.

Bruchez, M., M. Moronne, et al. (1998). "Semiconductor Nanocrystals as Fluorescent Biological Labels." Science **281**: 2013.

Chan, W. C. W. and S. Nie (1998). "Quantum Dot Bioconjugates for Ultrasensitive Nonisotopic Detection." Science **281**: 2016.

Colvin, V. L., M. C. Schlamp, et al. (1994). Nature **370**: 354.

Donega, C. d. M., S. G. Hickey, et al. (2003). J Phys. Chem. B **107**: 489.

Dubertret, B., P. Skourides, et al. (2002). Science **298**: 1759.

Dwarakanath, S., J. G. Bruno, et al. (2004). Biochem. Biophys. Res. Commun. **325**: 739.

Harrison, M. T., S. V. Kershaw, et al. (2000). Pure Appl. Chem. **72**: 295.

Henshaw, G., I. P. Parkin, et al. (1996). J.C.S. Chem. Commun.: 1095.

Hodes, G. (1993). Israel J. Chem. **33**: 95.

Huang, G. W., C. Y. Chen, et al. (2004). J Crystal Growth **265**: 250.

Kainthla, K. C., D. K. Pandya, et al. (1980). J. Electrochem. Soc. **127**: 1980.

Kim, J. H., D. Morikis, et al. (2004). Sensors Actuat. B **102**: 315.

Klimov, V. I., A. A. Mikhailovsky, et al. (2000). Science **290**: 314.

Lin, C. I., A. K. Joseph, et al. (2004). Biosen. Bioelectron. **20**: 127.

Michalet, X., F. F. Pinaud, et al. (2005). "Quantum dots for live cells, in vivo imaging and diagnostics." Science **307**: 583-544.

Murray, C. B., C. R. Kagan, et al. (2000). Annu. Rev. Mater. Sci. **30**: 545.

Murray, C. B., D. J. Norris, et al. (1993). "Synthesis and Characterization of nearly monodisperse CdE (E=S, Se, Te) Semiconductor Nanocrystallites." J. Am. Chem. Soc. **115**: 8706-8715.

Nemec, P., D. Mikes, et al. (2000). "Light-controlled growth of CdSe nanocrystalline films prepared by chemical deposition." Materials Science and Engineering **B69-70**: 500-504.

Peng, Q., Y. Dong, et al. (2001). Inorg. Chem. **40**: 3840.

Peng, X., L. Manna, et al. (2000). Nature **404**: 59.

Peng, Z. A. and X. Peng (2001). J Am. Chem. Soc. **123**: 183.

Qu, L. and X. Peng (2002). J Am. Chem. Soc. **124**: 2049.

Tessler, N., V. Medvedev, et al. (2002). Science **295**: 1506.

Wang, C., W. X. Zhang, et al. (1999). Mater Chem Phys **60**: 99.

Woggon, U. (1997). "Optical Properties of Semiconductor Quantum Dots."

Yan, Y. L., Y. Li, et al. (2003). "Preparation and characterization of CdSe nanocrystals via Na2SO3-assisted photochemical route." Mater Sci and Engineering **B103**: 202-206.

Chapter 4 Synthesis and Characterization of CdSe/CdS Core/Shell Quantum Dots

4.1 Introduction

High quality quantum dots have been prepared with advances in the modern colloid chemistry (Murray, Kagan et al. 2000; Qu, Peng et al. 2001). Because of the interesting size-tailored photoluminescence and strong resistance against photochemical reaction in solution, quantum dots have been widely used as bio-labels (Bruchez, Moronne et al. 1998; Chan and Nie 1998; Michalet, Pinaud et al. 2005). However, it is still an interest of researchers to boost the quantum yield (defined as the ratio of emission to absorption photons) and, thus, reduce the number of the quantum dots needed in the experiment. The atoms on the surface of a quantum dot act as defects since they are not fully bonded. Many of these defects are removed by being passivated with organic surfactants during certain synthesis process. Although up to 10% quantum yield (at room temperature) of these capped dots has been reported (Norris, Sacra et al. 1994), it remains as a challenge to passivate both anionic and cationic sites on the surface with organic ligands.

An alternative method to the use of organic molecules as surface passivation is to coat the surface with higher band gap inorganic semiconductor to form a core/shell structure. Not only are the dangling bonds of the core fixed by the shell, but the electron-hole pairs are more confined by the higher potential barriers as well. A variety of such core/shell nanostructure, CdSe/ZnS (Dabbousi, Rodriguez-Viejo et al. 1997), CdSe/ZnSe (Reiss, Bleuse et al. 2002), and CdSe/CdS (Peng, Schlamp et al. 1997) have been fabricated and improved photoluminescence quantum yield (up to 85%) has been reported.

Both ZnSe (2.72 ev) and CdS (2.42 ev) have higher band gap than that of CdSe (1.76 ev) and thus makes them good candidates as shell material. However, the larger lattice mismatch between ZnSe and CdSe (6.3%) makes CdS (3.9%) a better choice to be

the capping agent around the CdSe quantum dots. In this chapter, a description of the results obtained when CdSe/CdS core/shell QDs were synthesized. A thin layer of CdS crystal was grown on CdSe quantum dots, the latter were synthesized according to the description in Chapter 3, to form CdSe/CdS core/shell quantum dots. Both UV-Vis absorption and photoluminescence spectra of the CdSe/CdS solution were measured to characterize the core/shell system. In addition, X-ray diffraction (XRD) and TEM were performed to confirm the structure of the core/shell quantum dots.

4.2 Experiment Setup for CdS Coated CdSe Quantum Dots

CdSe quantum dots were prepared according to the synthesis process described in the previous chapter, with pH value of sodium selenosulfate at 7.2 and Cd^{2+} to Se^{2-} ratio of 4:1. Smaller Cd^{2+} to Se^{2-} ratio, instead of 6:1, was used out of concern for the toxicity of Cd^{2+} ions. To coat CdSe with CdS, a reaction chamber made of two three-necked flasks was set up as shown in Figure 4.1. The first flask (F1) was filled with certain amount of saturate sodium sulfide (Na_2S) solution. A syringe filled with 98% sulfuric acid (H_2SO_4) was stuck through a solid rubber stopper fitted in the middle opening of F1, with the other two openings fitted a single hole rubber stopper in which tubing was connected for a compressed nitrogen feed into F1 and to provide a connection to the second flask. 40ml of a solution containing 2nm CdSe quantum dot and 10ml of 10% isopropanol alcohol, which was used to prevent the formation of large bubbles due to the gelatin when nitrogen is carried through the QD solution, were injected in the second flask (F2), which was fitted with a solid stopper in the middle and two single hole rubber stoppers. Tubing to provide the gas intake from F1 was feed through one of the single hole stoppers with a glass tube that nearly touches the bottom of the flask, F2. A gas outlet was provided via tubing that as feed through the hole of the second single hole stopper. The end of tubing for the gas outlet was submerged in a beaker containing saturated sodium hydroxide (NaOH) solution to collect any additional gas that did not react.

First, the system was purged with nitrogen for several minutes to remove the

oxygen gas in flasks F1 and F2. Then, the sulfuric acid was injected into F1 drop by drop and reacted with sodium sulfide to generate hydrogen sulfide (H_2S), which was carried to the F2 by the nitrogen flow. The bubbles created by the nitrogen in F2 helped to agitate the CdSe solution so that hydrogen sulfide could react with the free Cd^{2+} ions and the CdSe QDs. The supply of hydrogen sulfide into F2 was regulated by the number of drops of sulfuric acid added to F1 and could be shut down by turning off the nitrogen regulator valve.

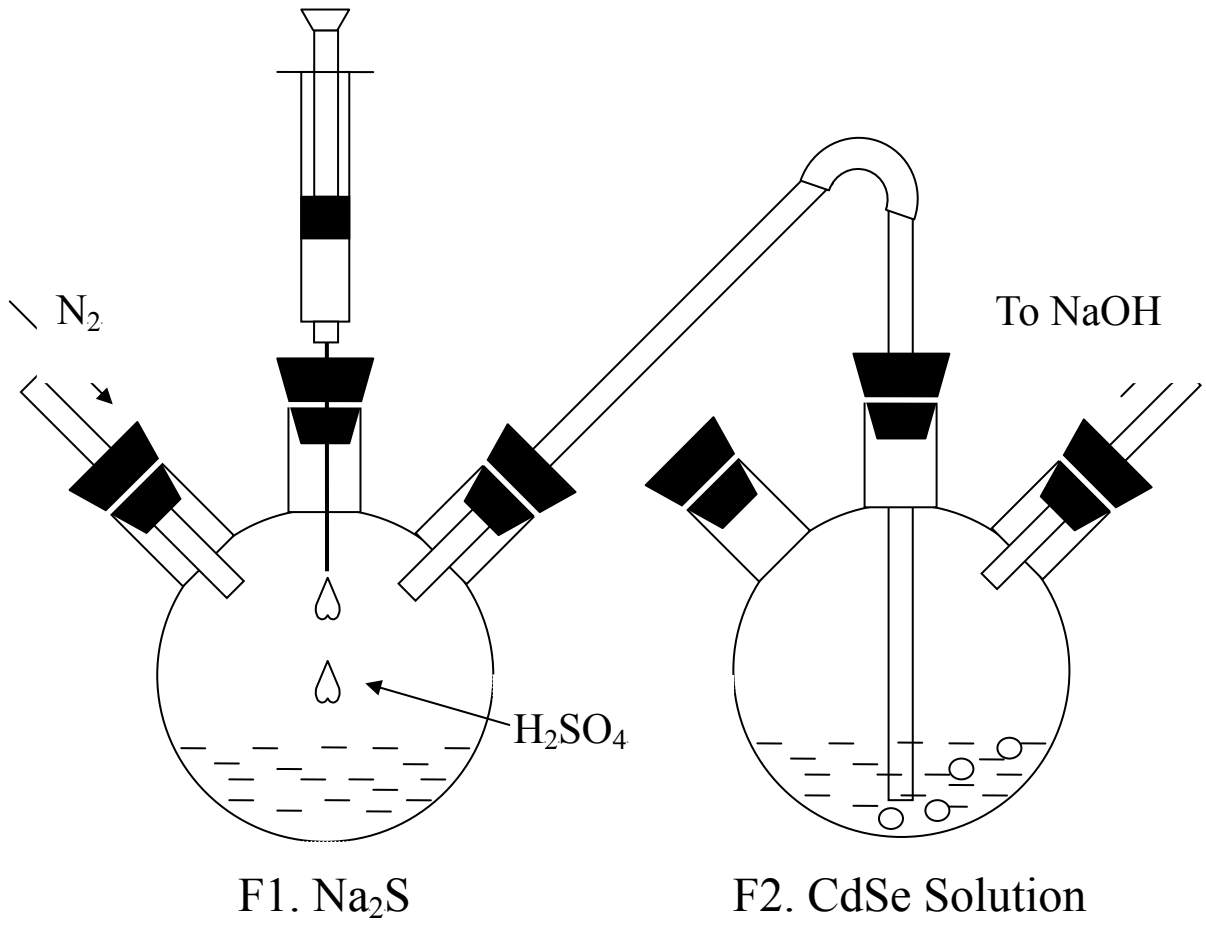

Figure 4.1 Experiment setup for synthesis of CdS coated CdSe quantum dots

4.3 Results and Discussion

After each drop of sulfuric acid was injected to the saturate sodium sulfide, the reaction chamber was purged with nitrogen for about 10-15 seconds. Then the second flask was well shaken for a minute and 3ml of the solution was taken out for absorption and photoluminescence (PL) measurement.

Figure 4.2 shows the photoluminescence spectra of CdSe and three CdSe/CdS samples with increasing shell thickness. In this figure, the black curve stands for the PL of CdSe bare dots and the red curve above it is the PL of CdSe/CdS where one drop of sulfuric acid had been added to F1. It is obvious that the intensity of PL was enhanced slightly with a thin CdS shell. The green curve represents the PL of CdSe/CdS dots with two drops of sulfuric acid added to F1. The peak intensity of PL from the CdSe QDs dramatically increased when coated with a CdS shell of this thickness. However, after one more drop of sulfuric acid was injected into F1, thus more hydrogen sulfide introduced into the CdSe/CdS solution, the interfacial defects generated as a result of the lattice mismatch between the CdSe and CdS began to quench the PL, shown as the blue curve. Since the motion of the photon-generated electrons extended into the CdS layer, which will be discussed later in this chapter, the slight shift of the PL peak (blue curve) to the longer wavelength is a result of the increase in the overall size of the core/shell quantum dot as more and more CdS grown on CdSe dots. As more hydrogen sulfide was carried into the CdSe/CdS solution, the PL from the CdSe core became almost undetectable; it was reduced by two orders of magnitude from that of the original CdSe solution. This is considered to be caused by the acidic environment due to the large amount of hydrogen sulfide present in the solution. As mentioned in Chapter 3, there were no QDs found in the acidic solution.

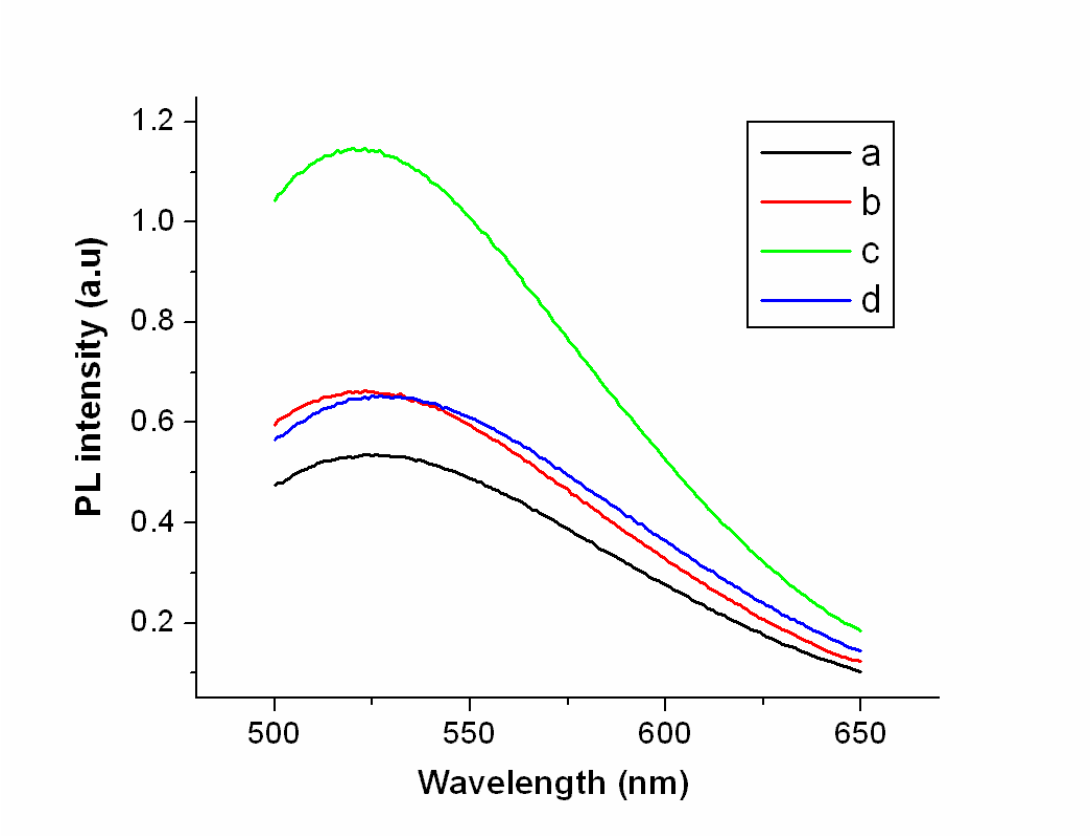

Figure 4.2 PL spectra of CdSe QDs (a) and CdSe/CdS with one drop (b) two drops (c) and three drops (d) of sulfuric acid injected into F1

The absorption spectra of corresponding solutions were shown in Figure 4.3. As can be seen, the overall shapes of the absorption spectra (black, red and green curves) remain the same with the absorption onset at about 450nm, which is the first exciton peak of CdSe. This is strong evidence that the CdS-only quantum dots were not formed during the shell growth process. Otherwise, an absorption onset near 370nm, the first exciton peak of CdS, should appear. The slightly broadening feature in the green curve indicates the size distribution of the core/shell structure was increasing as more sulfide ions were introduced. The blue curve, which correspond the absorption of CdSe with the thickest CdS shell in this series, is featureless in terms of absorption onset. This may be caused by the more crystal defects in CdSe quantum dots. The change in PL intensity was confirmed by repeating the experiments at least ten times. By comparing the optical spectra of CdSe/CdS solution to that of the 3ml sample withdrawn from the

solution one minute after the introduction of the hydrogen sulfide, it was found that the shell growth was completed no more than one minute after the hydrogen sulfide supply was shut off.

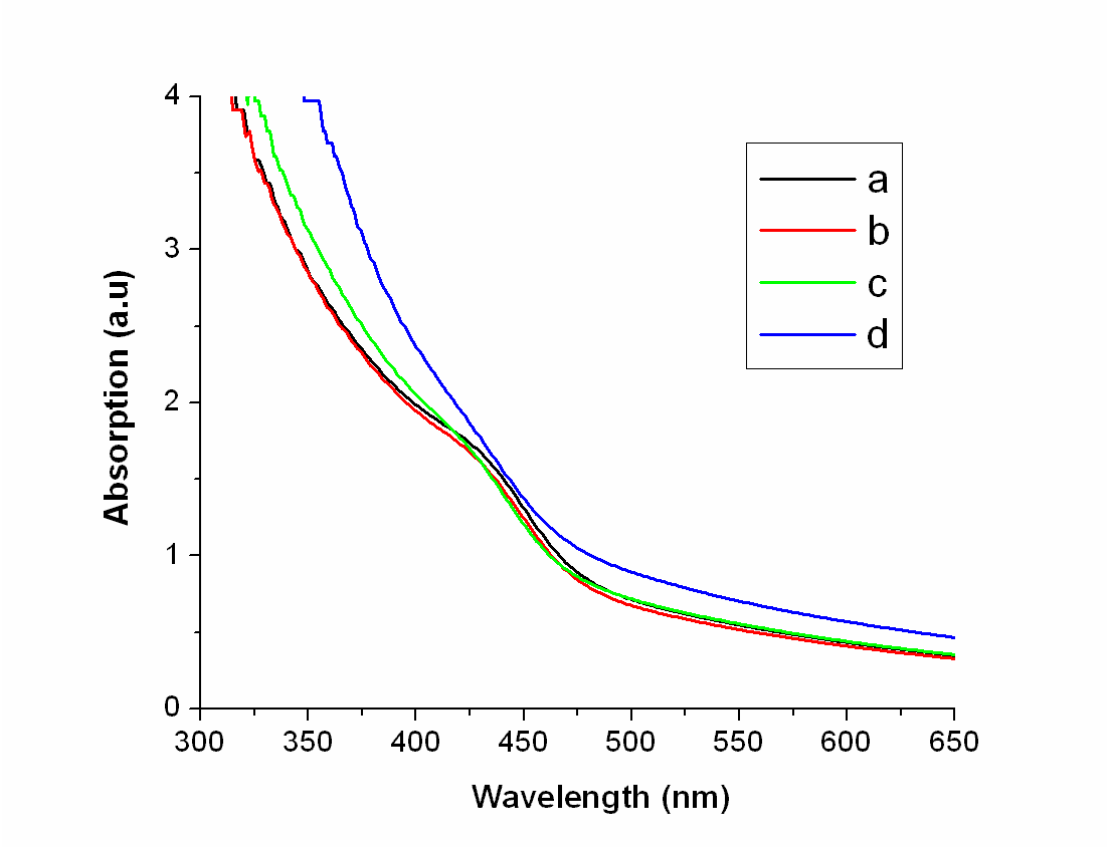

Figure 4.3 Absorption spectra of CdSe QDs (a) and CdSe/CdS with one drop (b) two drops (c) and three drops (d) of sulfuric acid injected into F1

A similar experiment was conducted and repeated for at least three times. It was found that if three times or more H_2S was used than that used to produce CdS coatings, CdS-only QDs were synthesized. This is believed to occur because the concentration of sulfur precursor increased above the nucleation threshold (Murray, Kagan et al. 2000). Three samples with CdS-only QDs were prepared by injecting three, six, and nine drops of sulfuric acid in F1, respectively. Figure 4.4 compares the absorption spectra of these samples with that of CdSe QDs. The first derivatives of the absorption spectra are shown in Figure 4.5.

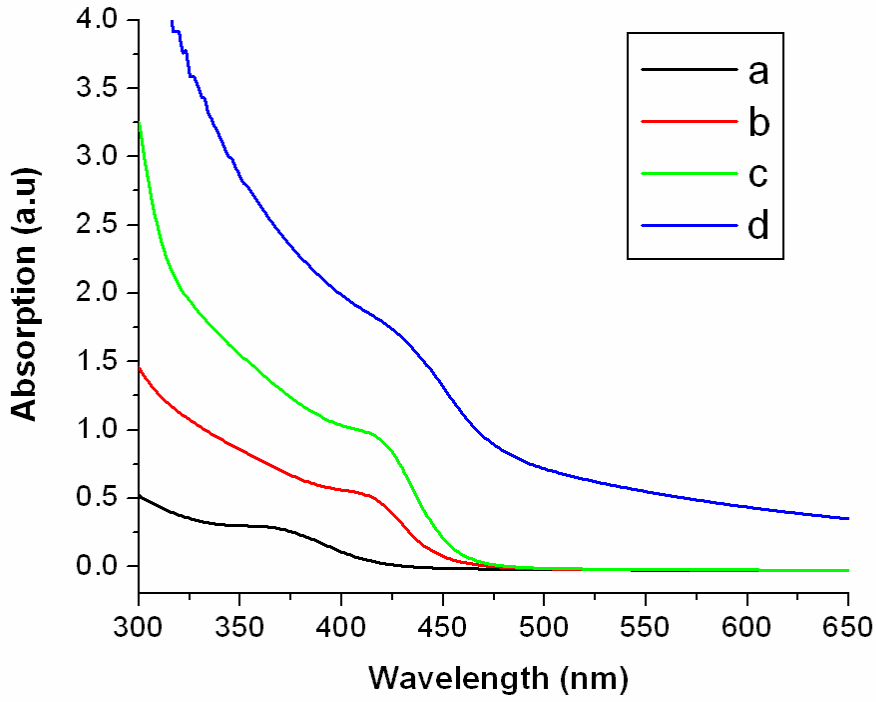

Figure 4.4 Absorption spectra of CdS-only QDs with three drops (a), six drops (b) and nine drops (c) of sulfuric acid injected into F1 and CdSe QDs (d)

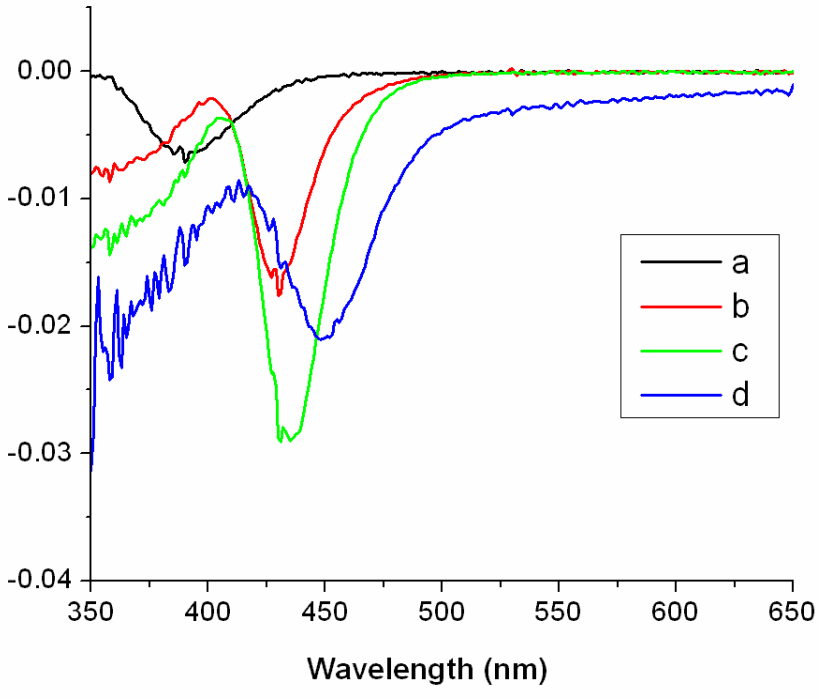

Figure 4.5 First derivatives of absorption spectra in Figure 4.4

When CdS-only quantum dots began to form in Cd^{2+} rich CdSe solution, the absorption spectra (black curve) showed an onset at 370nm which is the first exciton peak for the CdS QDs. As more hydrogen sulfide was present in the solution, larger CdS dots were grown as the absorption onsets (red and green curves) indicate with a shift from 370nm to 430nm of the exciton peak.

The wavelength that corresponds to the bulk band gaps of $CdSe_xS_{1-x}$ alloys can be calculated by equation (4-1) (Streckert and Ellis 1982)

$$\lambda(nm) = 508 + 210x \qquad (4\text{-}1)$$

where 508nm is the wavelength that corresponds to the bulk band gap of CdS and 210nm is the spectral difference between the bulk band gap of CdSe and CdS, so bulk alloy $CdSe_{0.5}S_{0.5}$ would have a band gap equivalent to 613nm. By analogy, quantum dots with nonzero molar ratio of S:Se would have an absorption onset at a smaller wavelength than 450nm, therefore the slight red-shift absorption onset shown in Figure 4.3 further proves the formation of CdSe/CdS core/shell structure instead of $CdSe_xS_{1-x}$ alloy dots. A TEM micrograph of CdSe/CdS quantum dots is shown below (Figure 4.6).

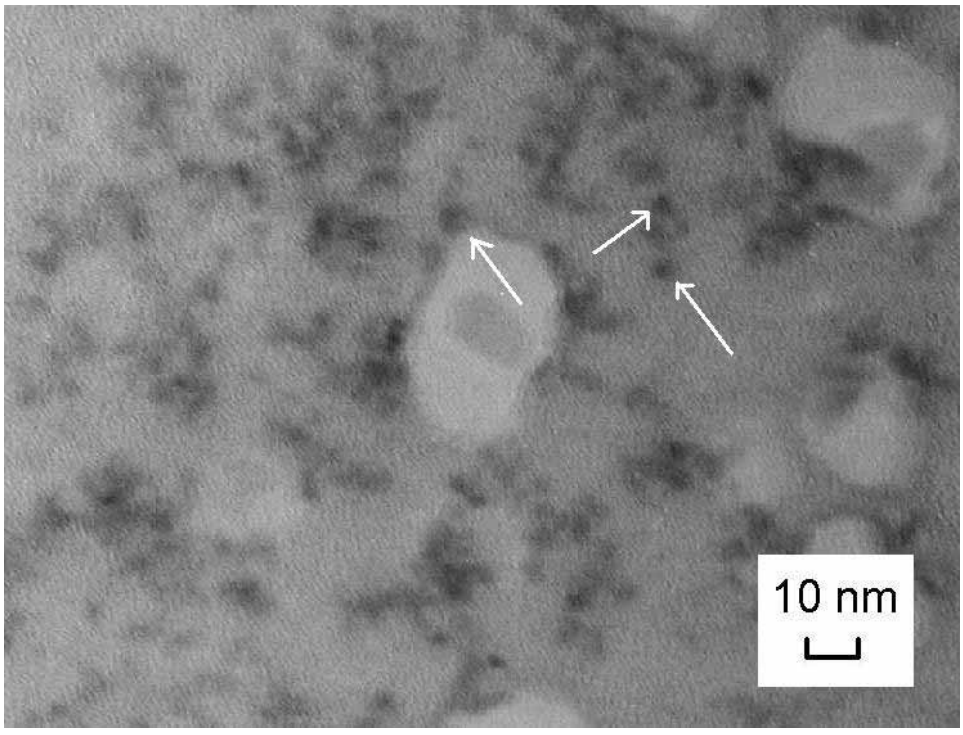

Figure 4.6 TEM micrograph of CdS coated CdSe quantum dots

X-ray diffraction (XRD) of the CdSe and CdSe/CdS quantum dots thin film, deposited on the glass slide, was performed on XDS 2000 (Scintac, Inc). The raw data are presented in Figure 4.7, where the background signal was from a clean slide, S1 was for CdSe QDs and S2 and S3 were from two CdSe/CdS core/shell samples, where QDs in S3 had a thicker CdS shell thickness than those in S2.

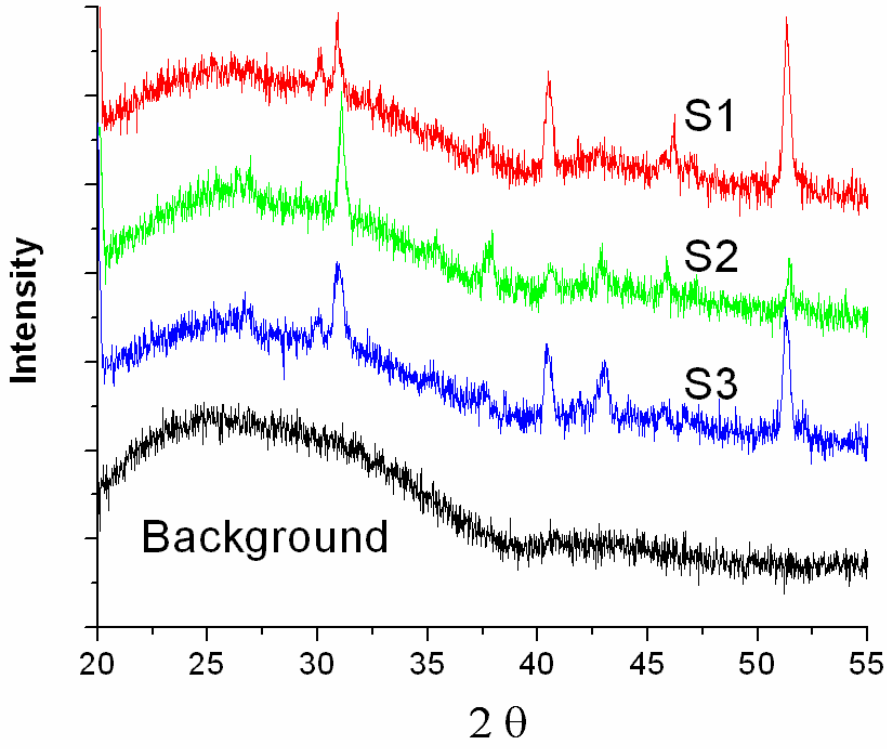

Figure 4.7 Raw XRD data of background from glass slide, CdSe (S1) and CdSe/CdS (S2 and S3, with increasing CdS thickness) samples

Figure 4.8 shows the normalized data, obtained by subtracting the background from S1, S2 and S3. All of three samples show wurtzite crystal structure (Murray, Norris et al. 1993). Since the characteristic diffraction angle of bulk CdS is a little bigger than those of CdSe, the slight peak shift to the right in diffraction angle around 32°

and 53° indicates the growth of CdS shell around CdSe dots.

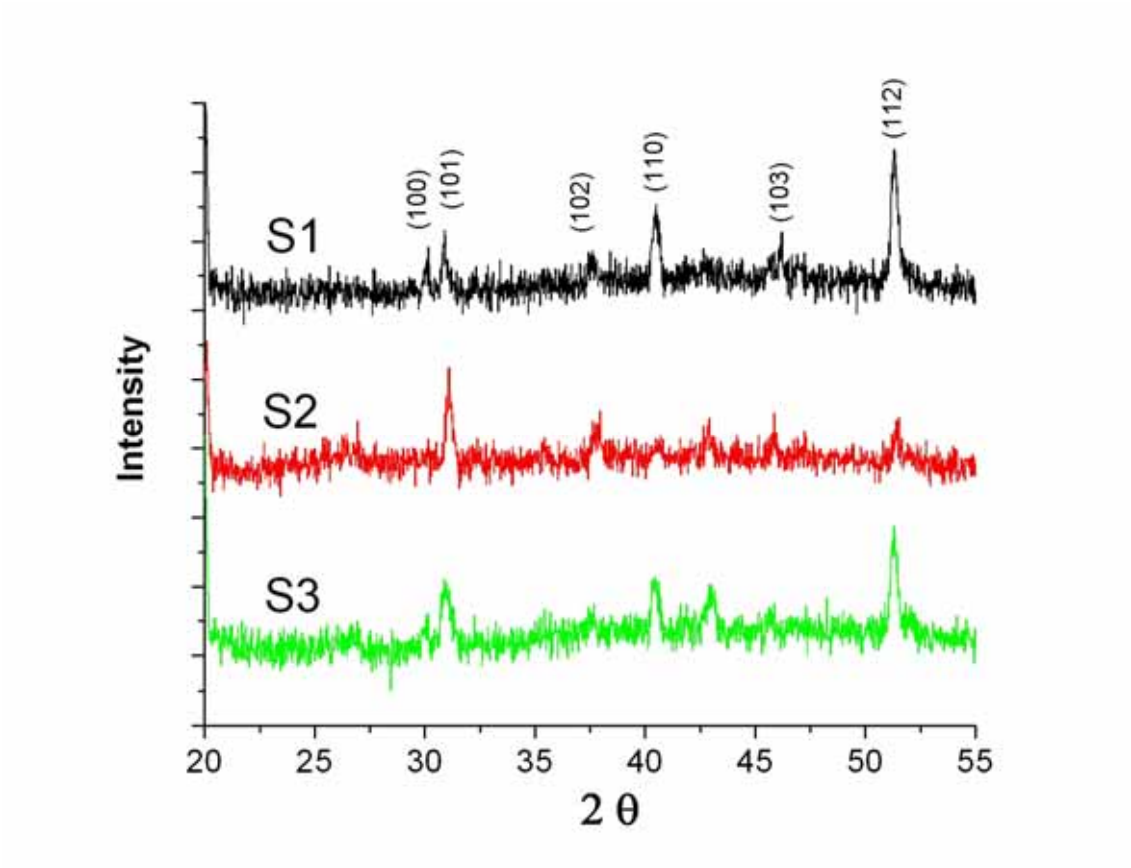

Figure 4.8 Normalized XRD data of CdSe (S1) and CdSe/CdS (S2 and S3) samples

Since the CdSe/CdS quantum dots that were synthesized in this study were core/shell structures instead composed of alloy composition, suggested by their optical properties, they have unique electronic levels, which can be understood with the "*particle in a sphere*" model discussed earlier in Chapter 2. The schematic energy levels of both CdSe and CdSe/CdS quantum dots are shown in Figure 4.9,

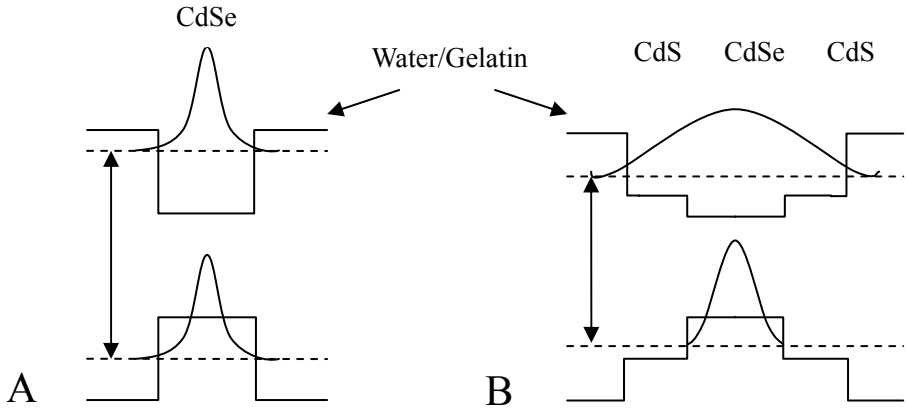

Figure 4.9 Schematic energy band structure of bare CdSe (A) and CdSe/CdS core/shell (B) quantum dots

where the dashed lines are electronic energy levels, between which are the absorption onsets for each type of dots. As suggested by the wavefunctions calculated with the "*particle in a sphere*" model (see Figure 4.9), the electrons are delocalized across the core/shell structure, while holes are confined mostly in the core area. So the slight red-shift of absorption peak as the CdS shell grown thicker can be explained by the reduced quantum confinement felt by the electrons, as if there was a bigger CdSe sphere as a result of the CdS capping. Because the surface states of CdSe DQs act as traps for photon-generated carriers, the enhanced photoluminescence of CdS-coated CdSe dots can be understood by the fact that the probability of radiative recombination increased due to the confinement of the holes in core area and the reduced interaction between surface, thus less nonradiative recombination, associated with surface states and crystal defects, took place (Franceschetti and Zunger 2000; Lifshitz, Glozman et al. 2000; Califano, Franceschetti et al. 2005).

4.4 Summary

Enhanced photoluminescence was achieved on CdS-coated CdSe quantum dots, known as CdSe/CdS core/shell nanocrystals. The thickness of the CdS shell is a crucial

factor in determining the optical properties of this core/shell system. If the CdS layer is too thin, the potential barriers for electrons and holes are not enough to prevent interactions of these carriers with surface states with the result that nonradiative recombination of a reasonable percentage of these carriers will take place. However, if the eptaxial growth of CdS is greater than a critical thickness and defects at the CdSe and CdS interface are created – likely misfit dislocations as a result of the lattice mismatch between CdSe and CdS, the photoluminescence will largely be quenched.

Although it is predicted by other groups that the CdS/CdSe system has enhanced photostability due to the confinement of holes, which is required at the surface during the photo-oxidation of selenium atoms (Katari, Colvin et al. 1994), more biocompatible and inert material as capping agent is required to render more robust quantum dots for biology and medical applications.

Reference

Bruchez, M. P., M. Moronne, et al. (1998). Science **281**: 2013.

Califano, M., A. Franceschetti, et al. (2005). "Temperature Dependence of Excitonic Radiative Decay in CdSe Quantum Dots: The Role of Surface Hole Traps." Nano Lett. **in print**.

Chan, W. C. W. and S. Nie (1998). "Quantum Dot Bioconjugates for Ultrasensitive Nonisotopic Detection." Science **281**: 2016.

Dabbousi, B. O., J. Rodriguez-Viejo, et al. (1997). "(CdSe)ZnS Core-Shell Quantum Dots: Synthesis and Characterization of a Size Series of Highly Luminescent Nanocrystallites." J Phys Chem B **101**: 9463.

Franceschetti, A. and A. Zunger (2000). "Optical transitions in charged CdSe quantum dots." Phys. Rev. B **62**: R16287-16290.

Katari, J. E. B., V. L. Colvin, et al. (1994). "X-ray Photoelectron Spectroscopy of CdSe Nanocrystals with Applications to Studies of the Nanocrystal Surface." J Phys Chem **98**: 4109-4117.

Lifshitz, E., A. Glozman, et al. (2000). "Optically Detected Magnetic Resonance Studies of the Surface/Interface properties of II-VI Semiconductor Quantum Dots." J Phys Chem B **104**: 10449-10461.

Michalet, X., F. F. Pinaud, et al. (2005). "Quantum dots for live cells, in vivo imaging and diagnostics." Science **307**: 583-544.

Murray, C. B., C. R. Kagan, et al. (2000). Annu. Rev. Mater. Sci. **30**: 545.

Norris, D. J., A. Sacra, et al. (1994). Phys. Rve. Lett. **72**: 2612.

Peng, X., M. C. Schlamp, et al. (1997). "Epitaxial Growth of Highly Luminescent CdSe/CdS Core/Shell Nanocrystals with Photostability and Electronic Accessibility." **119**: 7019.

Qu, L., Z. A. Peng, et al. (2001). "Alternative Routes toward High Quality CdSe Nanocrystals." Nano Lett. **1**: 333-337.

Reiss, P., J. Bleuse, et al. (2002). "Highly Luminescent CdSe/ZnSe Core/Shell Nanocrystals of Low Size Dispersion." Nano Lett. **2**: 781-784.

Streckert, H. H. and A. B. Ellis (1982). J. Phys. Chem. **86**: 4921.

Chapter 5 Synthesis of Silica Coated CdSe/CdS Core Shell Quantum Dots

5.1 Introduction

Unique size-tailored optical properties of inorganic nanocrystallites due to strong quantum confinement, especially CdSe, have drawn a great deal of attention of researchers and scientists for the past two decades. Many advantages over conventional organic fluorophore, such as broad absorption, narrow and symmetric emission (independent of excitation wavelength) and long emission lifetime, make the quantum dots possible as alternative biolabels and probes in biology and medical applications (Parak, Pellegrino et al. 2005). Since Murray's publication (Murray, Norris et al. 1993), utilizing the metal-organic precursor for the synthesis of CdSe nanocrystallites more than a decade ago, production of nearly monodispersed CdSe quantum dots have been greatly improved and been commercially available.

Higher band gap semiconductors have been utilized to coat these quantum dots to form core/shell structures in order to increase their quantum yield. The thin shell layer not only can passivate the dangling bonds and surface defects of quantum dots, thus decreasing the nonradiative pathway, but also can confine carriers, such as holes, more in the core region and away from the surface defects, therefore increasing the possibility of radiative recombination. Although 30-85% quantum yield at room temperature and increased photostability have been reported for core/shell structures via organometallic synthesis techniques, such as CdSe/ZnS (Hines and Guyot-Sionnest 1996; Dabbousi, Rodriguez-Viejo et al. 1997), CdSe/CdS (Peng, Schlamp et al. 1997) and CdSe/ZnSe (Reiss, Bleuse et al. 2002), biocompatibility and water-solubility are required to be able to use these high quality quantum dots in cells and tissues. Harnessing the thiolated molecules, which need a free carboxyl group facing the solution, onto the quantum dots surface is the major approach to make them hydrophilic (Chen, Yet et al. 1999; Mitchell, Mirkin et al. 1999). However, the bonds between the molecules and quantum dots are

dynamic, thus render a low stability of the dots in solution (Gerion, Pinaud et al. 2001). In addition, chemical reactions may lead to slow dissolving of the semiconductor material and releasing the toxic atoms to the environment. An alternative coating, which has to be biocompatible and more chemical robust, is necessary for use of the QDs in a harsh environment such as that found *in-vivo*.

Silica as coating material has been studied by many groups for the past few years (Correa-Duarte and M. Giersig 1998; Schroedter, Weller et al. 2002; Zhou, Kobayashi et al. 2004). Coating of quantum dots with a silica layer has many advantages. As a capping agent, silica coating is optically transparent and chemically inert, which increase the chemical stability and biocompatibility of the quantum dots. Moreover, the colloid chemistry of silica is well understood (Iler 1979; Bergna 1994) and many surface modification methods are available. Silica coatings have already been applied to CdTe (Schroedter and Weller 2002), CdS (Correa-Duarte, Giersig et al. 1998), and ZnS (Iler 1959) quantum dots and metal (Hardikar and Matijevic 2000) and polymer (Goller and Vincent 1998) colloidal particles.

In this chapter, a description of silica coating grown on CdSe/CdS quantum dots by surface silanization is presented. Photoluminescence of the silica-coated CdSe/CdS quantum dots showed a higher quantum yield after coating and TEM micrograph confirmed the new structure.

Also in this study, the measurement of the effect of a uniform static electric field, known as Stark effect, on the silica-coated CdSe/CdS quantum dots was conducted. A along with a discussion of electric field induced optical properties change is also included.

5.2 Experiment Details

Synthesis of silica encapsulated CdSe/CdS quantum dots

85wt% of mercaptopropyl trimethoxysilane (MPS) and 40% of sodium silicate were purchased from Acros Organics and Fisher Scientific, respectively.

The CdSe/CdS core/shell quantum dots were prepared as described in the previous chapter. Both MPS and sodium silicate were diluted with deionized (DI) water, to 0.13% and 0.6%, respectively. 0.1ml of this dilute solution of MPS was added to 10ml of CdSe/CdS solution, which was vigorously shaken for 15 minutes. This allows MPS to link with CdS shell through thiol/Cd bonds and to be ready for the deposition of silica coatings. Then 0.2ml of the 0.6% sodium silicate solution, which is naturally at pH value of 10, was added. After the solution was mixed well, the vial was kept in the dark at room temperature to allow the silica to gradually polymerize on the MPS-modified quantum dots. After several hours, 2ml of this solution was transferred to a vial filled with 8ml of 100% ethanol, a thicker silica coating were grown as a result of the precipitation of excessive silicate. Silica-coated CdSe/CdS dots precipitated out after having been mixed with ethanol. The solution containing the silica-coated CdSe/CdS QDs can be stored in the dark at room temperature for several months. If they were kept in the room light, these QDs would gradually degrade at a slower pace than those without silica coationgs.

A grid with samples of the silica-coated CdSe/CdS QDs was scanned using JEM-2000 FX II (JEOL) transmission electron microscopy (TEM) with an acceleration voltage of 200 kV and photoluminescence was measured by a home-made fluorescence spectrometer, assembled from two SPEX 1680 monochrometers and a photomultiplier tube as photon detector.

5.3 Characterization of Silica Coated CdSe/CdS Quantum Dots

Surface silanization is the growth of a glass shell around the particles. Since it is almost impossible to directly deposit a silica layer on the surface of CdS, the first step in the surface silanization of CdSe/CdS quantum dots is to bind (3-Mercaptopropyl) trimethoxysilane (MPS) molecules, as a primer layer, to the surface of the core/shell structures via thiol/Cd bonds. The methoxysilane groups ($Si\text{-}OCH_3$) hydrolyze into silanol groups (Si-OH) and become cross-linked, which stabilizes the silane layer on the CdSe/CdS surface. In the next step, the hydrophilic trimethoxysilane molecules, sodium

silicate, are added. By cross-linking the trimethoxysilane groups through the formation of siloxane bonds, the silica shell is connected with the primer layer. The initial silica layer formed in the solution allows the quantum dots transfer into ethanol without aggregation or Ostwald ripening (Mulvaney, Liz-Marza´n et al. 2000). The main advantage of surface silanization, compared to other procedures, such as mercaptopropionic acid (MPA) coatings (Chen, Yet et al. 1999; Mitchell, Mirkin et al. 1999), to stabilize quantum dots in aqueous solutions, is that the ligand layer providing water solubility is highly cross-linked and, therefore, extremely stable.

Two samples were prepared from one CdSe/CdS stock solution, one with 0.1 ml of 0.13wt% MPS and 0.2 ml of 0.6% sodium silicate (vial a in Figure 5.1) and the other with double this amount of MPS and sodium silicate (vial b in Figure 5.1). Three hours after the addition of MPS and sodium silicate, 2ml of solution from each vial were transferred into two new vials (c and d in Figure 5.1), which were filled with 8ml of 100% ethanol. Figure 5.1A shows how each of the CdSe/CdS solutions with silica coating appeared under room light a week after they were prepared; Figure 5.1B shows the same four vials under UV illumination, again a week after they had been prepared. It is clear that the PL efficiency of quantum dots decayed to zero even with a thin layer of silica after a week (vial a and b). Also, it is apparent that a thick silica coating, such as that on the QDs in vials c and d, is required to prevent, or at least slow down, reactions of the QDs with oxygen or other chemicals in the solution and any other degradation processes that reduce their radiative efficiency. The similar processes were repeated three times to confirm the results.

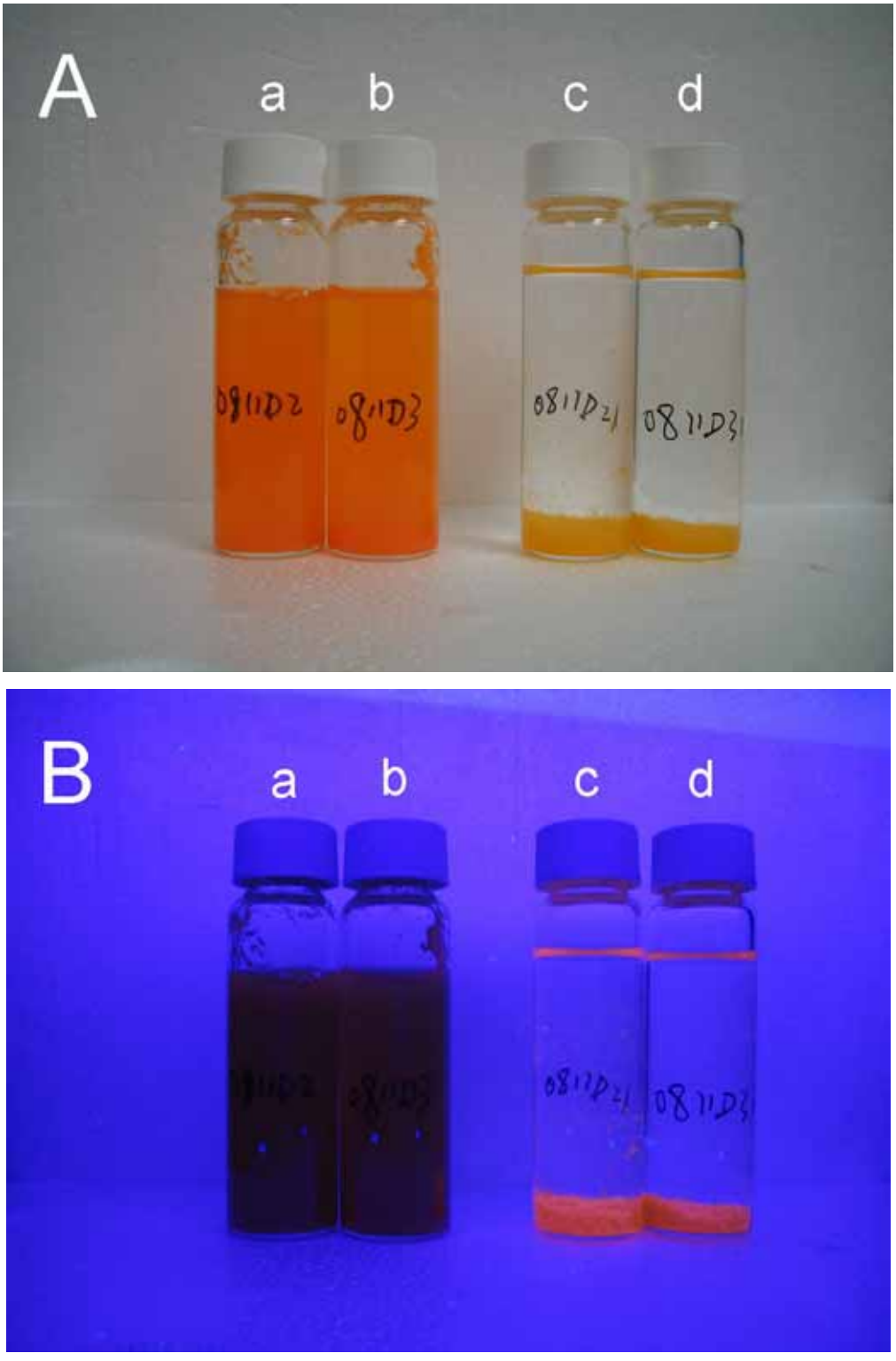

Figure 5.1 Silica coated CdSe/CdS solution under room light (A) and UV (B)

Photoluminescence of the silica-coated CdSe/CdS quantum dots from vial c and d are shown in Figure 5.2. The lower intensity of sample d compared to sample c is due to the fact that twice as much MPS was introduced in CdSe/CdS solution. This result is consistent with the fact that the presence of MPS has negative effect on the photoluminescence of quantum dots, reported by other groups (Rogach, Nagesha et al. 2000).

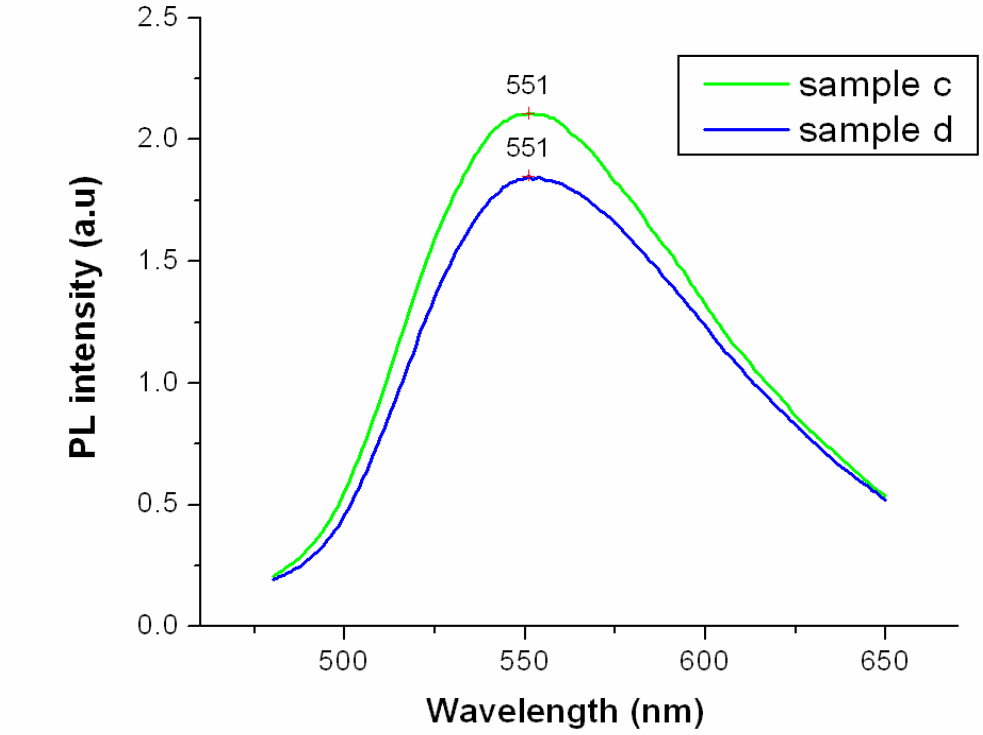

Figure 5.2 PL of sample c and d as a function of wavelength

A drop of sample c was dried on an ultra-thin carbon film-coated copper grid to prepare for a TEM scan. The micrograph (Figure 5.3) shows that multiple CdSe/CdS quantum dots were completely encapsulated in the silica matrix. The CdSe/CdS QDs appear to be randomly distributed within the silica matrix; there was no aggregation of

quantum dots inside the matrix due to the silica coating. The silica-coated CdSe/CdS quantum dot clusters were on the order of 15-20 nm in diameter.

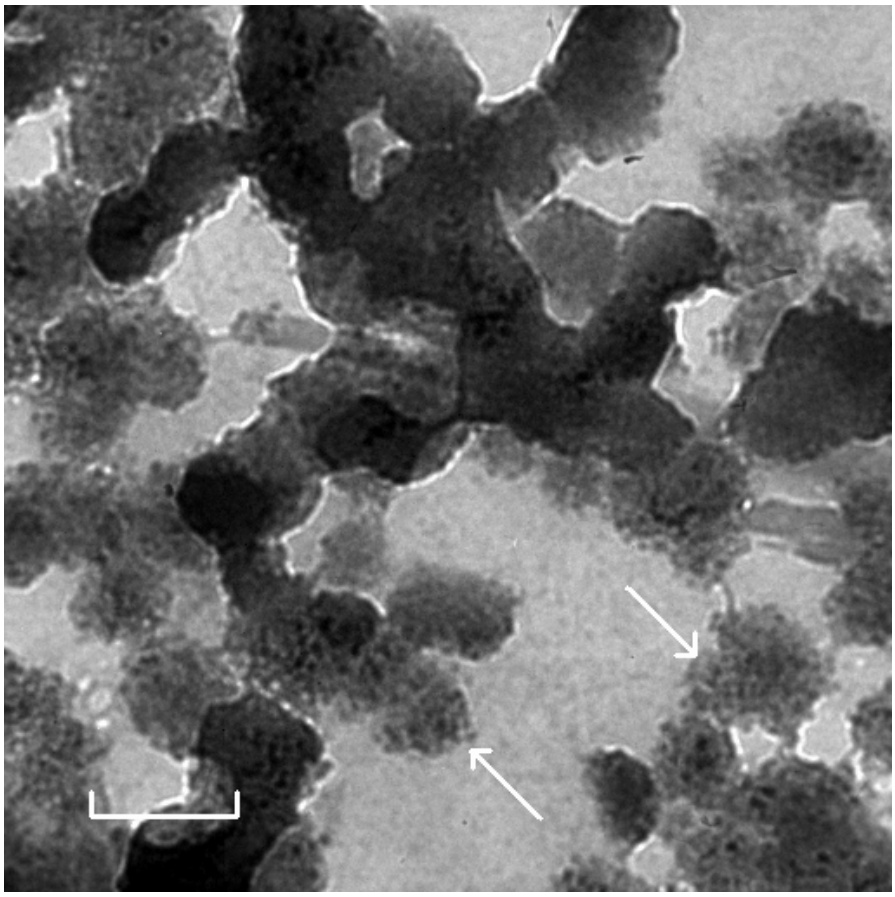

Figure 5.3 TEM micrograph of sample c, the length of the microbar represents 20 nm

5.4 Quantum Confined Stark Effect of Silica Coated CdSe/CdS Quantum Dots

Motivated by novel electro-optical devices, the effects of an applied electric field on confined carriers and excitons, known as quantum confined Stark effect (QCSE), have been extensively investigated both experimentally and theoretically for semiconductor

quantum wells two decades ago (Bastard, Mendez et al. 1983; Miller, Chemela et al. 1984; Miller, Chemela et al. 1985). The electric field dependence of the GaAs-$Al_xGa_{1-x}As$ quantum well's optical absorption was studied by Miller et al. and a red-shift of the exciton energy, which is due to the polarization of electron-hole pairs induced by the applied electric field, was observed. An increase in the exciton recombination lifetime under electric field was also reported, which is interpreted as a result of decreasing of the electron and hole wavefunction overlap (Köhler, Polland et al. 1988).

Since it provides a better understanding of the electronic structure of quantum dots, QCSE have also been explored for semiconductor nanocrystallites. Dissanyake et al. (Dissanyake, Lin et al. 1995) studied quantum confined Stark effect on exciton recombination lifetime in $CdS_{1-x}Se_x$ quantum dots embedded in a glass matrix by time-resolved photoluminescence spectroscopy. It was also found that the exciton recombination lifetime increased, due to the same reason for quantum wells. QCSE in single CdSe quantum dot was investigated by Empedocles and Bawendi (Empedocles and Bawendi 1997) and Stark shifts of the lowest excited state by more than two orders of magnitude than the PL linewidth were observed.

From the theoretical point of view, Hache et al. (Hache, Richard et al. 1989) used the independent model, which neglected the Coulomb interaction between electron and hole, with infinite barrier, where the quadratic field dependence of the line-shift was explained by the second order perturbation theory. The Coulomb potential was adopted by Ekimov et al. (Ekimov, Efros et al. 1990) who calculated the problem in the intermediate confinement model. Normura and Kobayashi (Normura and Kobayashi 1990), who included both the Coulomb and surface polarization energy, utilized a variational method to calculate the ground state exciton energy due to the applied electric field. Chen et al. (Chen, Wen et al. 1995) applied a numerical matrix-diagonalization approach to calculate the energy levels and wavefunctions of ground and several excited states of excitons in CdS and $CdS_{1-x}Se_x$ quantum dots.

In this study, the electrical field dependent photoluminescence of the silica-coated CdSe/CdS quantum dots was studied to have a better understanding of their optical properties as well as the effect of the binding events of the functionalized QDs on the PL

wavelength and intensity. Due to the applied electric field strength and complications of the quantum dots system under investigation, a simple calculation from perturbation theory was conducted to match the experimental results.

5.4.1 Quantum Confined Stark effect Measurement Setup

The precipitate that was formed upon adding ethanol to the solution containing silica-coated CdSe/CdS quantum dots was dropped on a piece of polyvinyl chloride (PVC) film (2cm x 1cm, 0.0025cm thick) and allowed to dry at room temperature for an hour. A transparent thin film composed of the silica-coated CdSe/CdS quantum dot was formed after the water and ethanol evaporated. Then, the PVC film was folded in half (see Figure 5.4) and placed between two slides. Each slide had one surface coated with indium tin oxide (ITO). When the two slides were in contact with the PVC film, the ITO-coated side of each slide faced the PVC film. Electrical connections to the DC power supply were made by two alligator clips, which were clamped on an exposed ITO portion of each slide. By applying DC voltages from 0 to 2kV, electric fields of up to $4x10^5$ V/cm were created between the two slides.

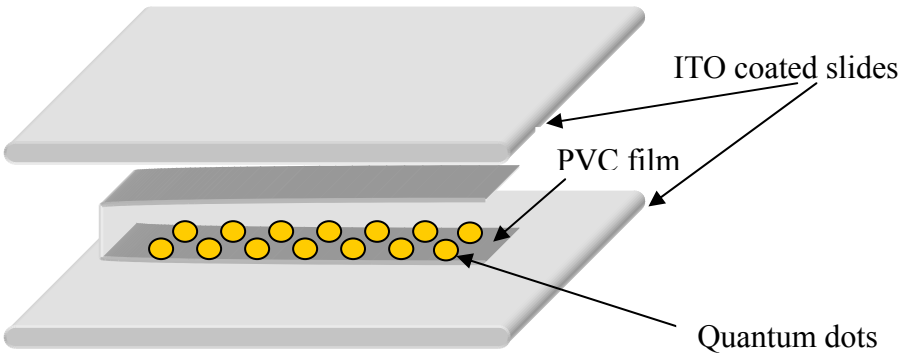

Figure 5.4 Sample preparations for stark effect measurement

The whole fixture was mounted on a fixed filter holder. A UV (370nm) LED illuminated the quantum dots in a direction along lengths of the slides and the fluorescence was detected at a 90° angle to the optical axis of the illumination source using a 0.5m monochrometer (SPEX 1680) with a photomultiplier tube attached, as schematically shown in Figure 5.5.

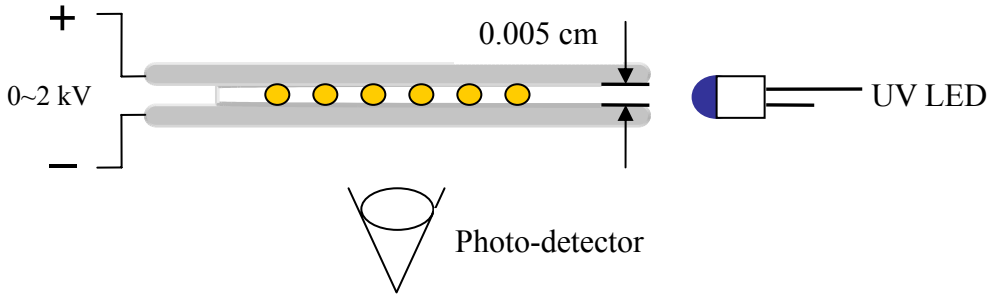

Figure 5.5 Experiment setup for Stark effect measurement

5.4.2 Result and Discussion

The photoluminescence spectra of silica-coated CdSe/CdS quantum dots under the influence of different electrical field strengths are shown in Figure 5.6. As the DC power supply gradually increased from zero to 1kV and 2kV, a slightly enhanced photoluminescence was observed with a visible blue-shift of the PL peak. The changes of both intensity and peak of the PL were reversible when the power supply was adjusted from 2kV back to zero.

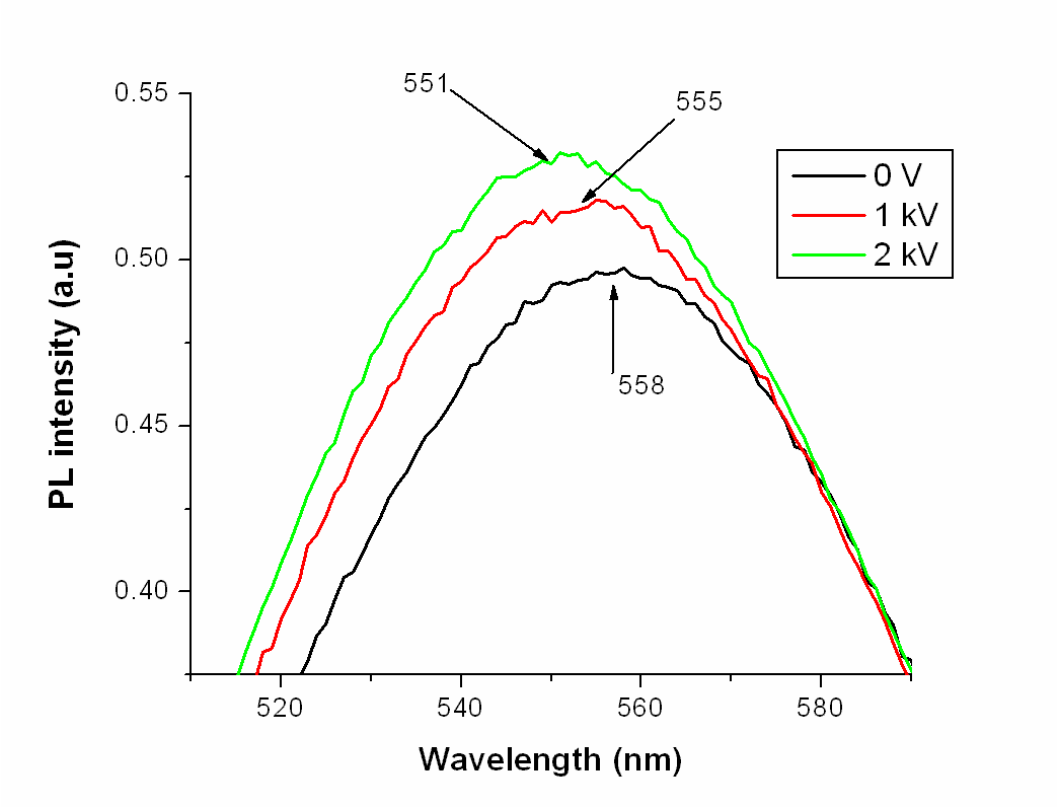

Figure 5.6 PL intensity as a function of wavelength under different applied electrical field

For a simple theoretical treatment of this experiment, let us consider a carrier, with charge e and effective mass m^*, in an infinite potential well of width a (in this case, it is the average diameter of the quantum dots) in the presence of an electric field, F, along the direction of the well. The Hamiltonian of this problem is (Bastard, Mendez et al. 1983)

$$H = H_0 + |e|Fz \tag{5-1}$$

where H_0 is the Hamiltonian with zero electric field. For weak fields, which satisfy

$$|e|Fa << h^2/2m^* a^2 \tag{5-2}$$

a second-order perturbation gives the energy shift of the ground state (Fernandez and Castro 1982)

$$\Delta E = -C_{pert} m^* e^2 F^2 a^4 / \hbar^2 \tag{5-3}$$

with

$$C_{pert} = \frac{1}{24}\pi^2\left(\frac{15}{\pi^2} - 1\right) \tag{5-4}$$

Since there is a uniform silica coating around the quantum dots, the electric field felt by the dots is reduced to (Magid 1972)

$$F_d = \left(\frac{3\varepsilon_g}{\varepsilon_d + 2\varepsilon_g}\right) F_a \tag{5-5}$$

where F_a is the applied electric field and ε_g and ε_d are dielectric constant of silica and CdSe, respectively.

Table 5-1 lists the parameters used to calculate the energy shifts of ground states for both electrons and holes.

Table 5.1 Constants Used to Calculate Energy Shifts

m_e*	m_h*	ε_g	ε_d	a (nm)
0.11	2.5	3.8	9.8	3.0

Table 5.2 compares the calculated ($\Delta E_{e,h}$ for electrons and holes) and experimental energy (ΔE^+ and ΔE^- represent the PL peak shifts before and after the electrodes were switched, respectively) shifts in meV.

Table 5.2 Calculated vs. Experimental Energy

	ΔE_e	ΔE_h	ΔE^+	ΔE^-
0 to 1kV	-0.11	2.51	1.91	1.89
0 to 2kV	-0.176	4.01	4.50	4.43

The Stark shifts as a function of electric field can be fitted by (Empedocles and Bawendi 1997)

$$\Delta E = \mu\xi + 0.5\alpha\xi^2 + \ldots \quad (5\text{-}6)$$

where ξ is applied electric field and μ and α are excited state dipole and polarizability, respectively. Since the size and orientation of the quantum dots in the silica matrix are quite random, the average of overall dipole component goes to zero, leaving the energy transition a quadratic shift (see Figure 5.7).

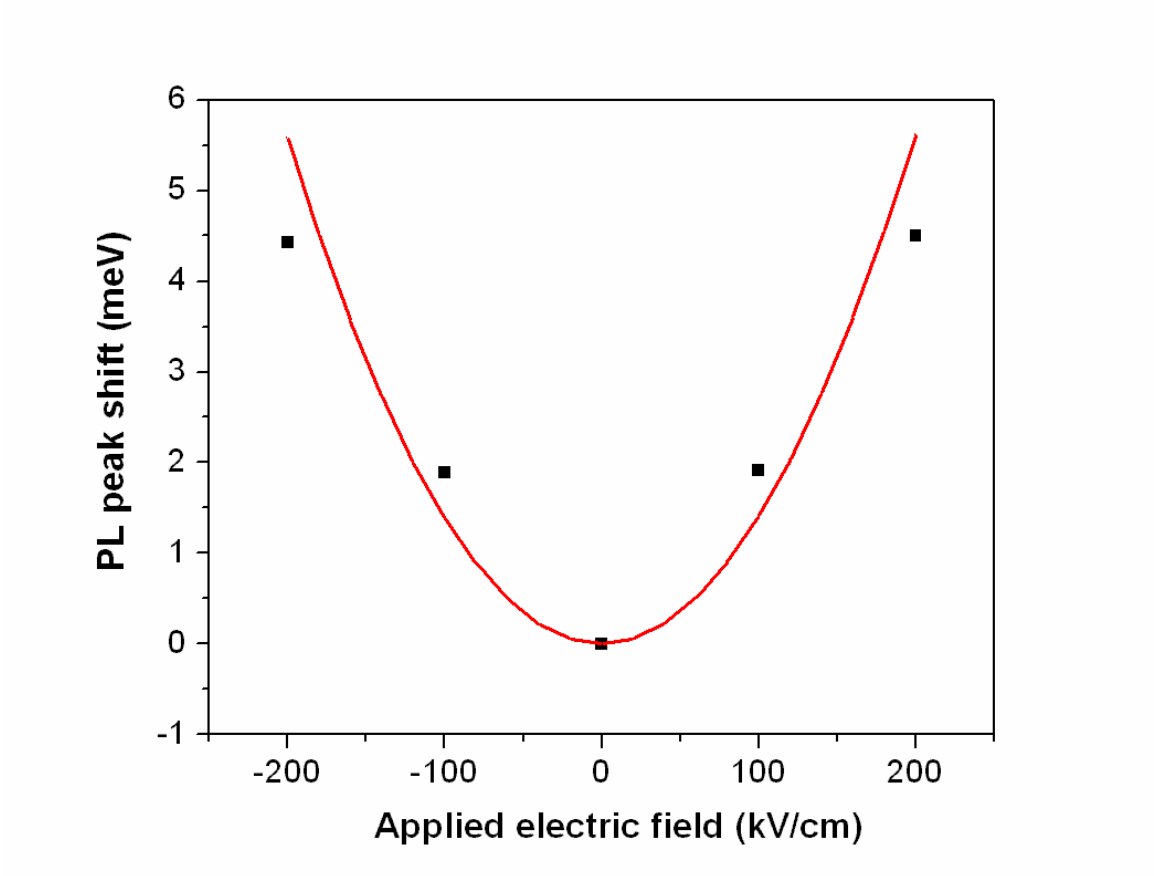

Figure 5.7 PL peak shift as a function of applied field where the closed squares are the measured shift and the red curve is the quadratic fit of the data

Although the quantum yield of the dots would decrease due to the increasing

exciton recombination lifetime under the applied field, there are other processes that might enhance the photoluminescence of the quantum dots. The applied electric field changes the distribution of charges in the quantum dots by polarizing the energy state. This can affect the coupling between the excitons and phonons. Therefore, a dark exciton, or optically prohibited electron-hole pair recombination at zero field, could emit light by involving a phonon assisted transition (Sercel and Vahala 1990; Vahala and Sercel 1990; Norris, Sacra et al. 1994).

5.5 Summary and future work

CdSe/CdS core/shell quantum dots were coated by a silica layer through a surface silanization approach. The structure of multiple dots embedded in the silica matrix without aggregations was confirmed by TEM micrographs. Quantum confined Stark effect was studied in these silica-coated quantum dots by applying up to 400 kV/cm electric field. A blue shift with slightly enhanced PL peak was observed with increasing the electric field. The reason for the asymmetric enhancement of the PL is not clear.

The silica coating greatly improved the photostability of the quantum dots compared to the ones without this coating or with a too thin coating. Additionally, these dots are considered more biocompatible, which has to be proved by further *in-vivo* feasibility study.

The quantum dot synthesis technique and silica coating method described in this study will benefit the future work for quantum dots of other compositions. It was recently confirmed that the emission spectra of the quantum dots in present study overlap the emission of the biological system in which the quantum dots are to be incorporated. Thus, quantum dots with longer emission wavelength, CdTe (whose emission extends into near-IR) for instance, are needed.

Reference

Bastard, G., E. E. Mendez, et al. (1983). "Variational calculations on a quantum well in an electric field." Phys. Rev. B **28**: 3241-3245.

Bergna, H. E. (1994). "The Colloid Chemistry of Silica." 234.

Chen, Z., G. W. Wen, et al. (1995). "Quantum-confined Stark effects in semiconductor quantum dots." Phys. Rev. B **52**: 5913-5922.

Correa-Duarte, M. A., M. Giersig, et al. (1998). Chem. Phys. Lett. **286**: 497.

Dabbousi, B. O., J. Rodriguez-Viejo, et al. (1997). "(CdSe)ZnS Core-Shell Quantum Dots: Synthesis and Characterization of a Size Series of Highly Luminescent Nanocrystallites." J Phys Chem B **101**: 9463.

Dissanyake, A. S., J. Y. Lin, et al. (1995). "Quantum-confined Stark effects in $CdS_{1-x}Se_x$ quantum dots" Phys. Rev. B **51**: 5457-5460

Ekimov, A. I., A. L. Efros, et al. (1990). J. Lum. **46**: 97.

Empedocles, S. A. and M. G. Bawendi (1997). "Quantum-confined Stark effect in single CdSe nanocrystallite quantum dots." Science **278**: 2114.

Fernandez, F. M. and E. A. Castro (1982). Physica (Utrecht) **11A**: 334.

Gerion, D., F. Pinaud, et al. (2001). "Synthesis and Properties of Biocompatible Water-Soluble Silica-Coated CdSe/ZnS Semiconductor Quantum Dots." J. Chem. Phys. B. **105**: 8861-8871.

Goller, M. I. and B. Vincent (1998). Colloids Surf. **142**: 281.

Hache, F., D. Richard, et al. (1989). Applied Physics Letters **55**: 1504.

Hardikar, V. V. and E. J. Matijevic (2000). Colloid Interface Sci. **221**: 133.

Hines, M. A. and P. Guyot-Sionnest (1996). "Synthesis and Characterization of Strongly Luminescing ZnS-Capped CdSe Nanocrystals." J Phys Chem **100**: 468.

Iler, R. K. (1959). **U.S. Patent 2,885,366**.

Iler, R. K. (1979). "The Chemistry of Silica: Solubility, Polymerization, Colloid and Surface Properties and Biochemistry of Silica."

Köhler, K., H. J. Polland, et al. (1988). "Photoluminescence of two-dimensional excitons in an electric field: Lifetime enhancement and field ionization in GaAs quantum wells." Phys. Rev. B **38**: 5496.

Magid, L. M. (1972). "Electromagnetic Fields, Energy and Waves." p350-370.

Miller, D. A. B., D. S. Chemela, et al. (1985). "Electric field dependence of optical absorption near the band gap of quantum-well structures." Phys. Rev. B **32**: 1043.

Miller, D. A. B., D. S. Chemela, et al. (1984). "Band-edge electroasorption in quantum well structures: the quantum confined Stark effect." Phys. Rev. Lett. **53**: 2173.

Mulvaney, P., L. M. Liz-Marza´n, et al. (2000). J. Mater. Chem **10**: 1259.

Murray, C. B., D. J. Norris, et al. (1993). "Synthesis and Characterization of nearly monodisperse CdE (E=S, Se, Te) Semiconductor Nanocrystallites." J. Am. Chem. Soc. **115**: 8706-8715

Normura, S. and T. Kobayashi (1990). Solid state commun. **74**: 1153.

Norris, D. J., A. Sacra, et al. (1994). "Measurement of the size dependent hole spectrum in CdSe quantum dots." Phys. Rve. Lett. **72**: 2612.

Parak, W. J., T. Pellegrino, et al. (2005). "Labeling of cells with quantum dots." Nanotechnology **16**: R9-25.

Peng, X., M. C. Schlamp, et al. (1997). "Epitaxial Growth of Highly Luminescent CdSe/CdS Core/Shell Nanocrystals with Photostability and Electronic Accessibility." **119**: 7019.

Rogach, A. L., D. Nagesha, et al. (2000). Chem. Mater. **12**: 2676.

Schroedter, A. and H. Weller (2002). "Biofunctionalization of Silica-Coated CdTe and Gold Nanocrystals." Nano Letters **2**: 1363-1367.

Sercel, P. C. and K. J. Vahala (1990). "Analytical formalism for determining quantum-wire and quantum-dot band structure in the multiband envelope-function approximation." Phys. Rev. B **42**: 3690-3710.

Vahala, K. J. and P. C. Sercel (1990). "Application of a total-angular-momentum basis to quantum-dot band structure." Phys. Rev. Lett. **65**: 239-242.

Zhou, X., Y. Kobayashi, et al. (2004). "Preparation of silica encapsulated CdSe quantum dots in aqueous solution with the improved optical properties." Applied Surface Science **242**: 281-286.

Chapter 6 Engineering Significance

Since common cells are almost transparent, they can hardly be seen by human eyes under optical microscope. Researchers often rely on certain fluorescence material, which attach to the interested biological component, in order to detect cell activities. Although organic fluorescent dye has been widely used to label the cells, their drawbacks, such as narrow absorption band and high chemical reactivity, are obvious compared to the nanomaterial counterparts, quantum dots (QDs), especially CdSe, whose emission spectra spread most of the visible wavelengths. Both biocompatibility and aqueous solubility are required for QDs to be used in biological system. Because CdSe QDs synthesized through metal-organic approach are hydrophobic, ligands exchange or extra coating are needed for those dots to use in aqueous environment. In addition, highly toxic metalorganic precursors make this complex process much less desirable than the method under development here are, which offers an easy and user-friendly way to prepare high quality CdSe QDs.

CdSe/CdS core/shell structure QDs were synthesized to significantly enhance the PL intensity from CdSe so that much less QDs are needed to inject into cells to obtain strong signals. Silica coatings were also developed on the core/shell QDs to increase chemical stability and biocompatibility of the QDs. Silica coatings are also easy to functionalize by conjugating with various molecules, which can be used to track the cell activities or chemical pathways inside cells. It has been reported that PL intensity and peak wavelength of the QDs could change upon chemical bonding events of the functional molecules. The electric charges change, among others, is considered to contribute to this process. Therefore, the effect of an applied electric field, known as Stark effect, on the PL intensity and wavelength of the QDs was studied to give preliminary understanding of such phenomenon.